Journal of Molecular Liquids 424 (2025) 127119

Contents lists available at ScienceDirect

Journal of Molecular Liquids

journal homepage: www.elsevier.com/locate/molliq

Interfacial and self-association behaviour of poloxamer 188 in aqueous solutions

Lukas Bollenbach [a], Marie-Luise Trutschel [a], Stefan Gröger [b], Patrick Garidel [c,d], Karsten Mäder [a,*]

[a] Martin-Luther-University Halle-Wittenberg, Institute of Pharmacy, Faculty of Biosciences, Wolfgang-Langenbeck-Strasse 4, 06120 Halle (Saale), Germany
[b] Martin-Luther-University Halle-Wittenberg, Institute of Physics, Faculty of Natural Sciences II, Betty-Heimann-Str. 7, 06120 Halle (Saale), Germany
[c] Boehringer Ingelheim Pharma GmbH & Co. KG, Innovation Unit, PDB-TIP, Birkendorfer Straße 65, 88397 Biberach an der Riss, Germany
[d] Martin-Luther-University Halle-Wittenberg, Institute of Chemistry, Faculty of Natural Sciences II, Von-Danckelmann-Platz 4, 06120 Halle (Saale), Germany

ARTICLE INFO

Keywords:
Poloxamer 188
Critical micelle concentration
Surface tension
Fluorescence spectroscopy
Electron paramagnetic resonance
Nuclear magnetic resonance

ABSTRACT

Poloxamer 188 plays a vital role as an excipient in the pharmaceutical industry. It is used as a solubiliser, wetting agent, shear protectant and stabiliser in protein and viral vector formulations. In this work, we characterise poloxamer 188s micelle formation characteristics using surface tension measurements to investigate the interfacial behaviour. In addition, differential scanning calorimetry was used to monitor unfolding processes at increasing temperatures. The size of the surfactant association was followed by dynamic light scattering, and fluorescence spectroscopy was used to get insights into the formation of a hydrophobic compartment by poloxamer 188 micelles. Additionally, electron paramagnetic resonance spectroscopy provided information about micro-viscosity and polarity. Nuclear magnetic resonance spectroscopy (^{1}H and ^{13}C) complemented the set of methods by providing data on the chemical environment of the polymer blocks. Poloxamer 188 concentrations up to 160 mg·mL^{-1} were investigated at temperatures between 5 °C to 80 °C. A strong dependency on temperature and solutes in surfactant solutions was found, conditional on their influence on the association behaviour in aqueous solution. We conclude that poloxamer 188 does not form micelles under conditions relevant to pharmaceutical formulation as a function of surfactant concentration, temperature and buffer system. The suspected reason for this is the very high hydrophilicity of the poloxamer molecule and the strong temperature dependence of the polyethylene oxide content in particular. Poloxamer 188 becomes increasingly lipophilic to show micelle formation only at increased temperature or in the presence of specific trehalose concentrations. These results provide insight into the characteristics of poloxamer 188 in aqueous solutions, allowing the stabilisation properties of drugs in drug delivery systems to be elucidated.

1. Introduction

Poloxamers are tri-block copolymers with a central hydrophobic polypropylene oxide (PPO) unit flanked by two polyethylene oxide (PEO) blocks. This amphiphilic character gives poloxamers surface-active properties and the ability to interact with interfaces [1–3]. Due to these properties, poloxamers are well-established excipients in the pharmaceutical industry. Applications include oral forms such as tablets, capsules, solutions, and suspensions, topical or ophthalmic products like gels and creams, and liquids for parenteral medicines. In addition to their use as excipients in dosage forms, poloxamers play a key role in biotechnology as shear and interface stabilisers for cells,

Abbreviations: A_N, Nitrogen isotropic hyperfine coupling constant (Distance of the outer signals in EPR); CMC, Critical micelle concentration; CMCR, Critical micelle concentration range; CMT, Critical micelle temperature; CPS, Counts per second (Fluorescence); DLS, Dynamic light scattering; DSA, Drop shape analysis; DSC, Differential scanning calorimetry; EPR, Electron paramagnetic resonance spectroscopy; HLB, Hydrophilic-lipophilic-balance; I_1, Intensity at first emission maximum of Pyrene; I_3, Intensity at third emission maximum of Pyrene; ITC, Isothermal titration calorimetry; logP, decadic logarithm of the n-octanol–water partition coefficient; NMR, Nuclear magnetic resonance spectroscopy; P188, Poloxamer 188; PEO, polyethylene oxide; PPO, polypropylene oxide; T, Temperature; τ_c, Rotational correlation time (EPR); Tempol, 4-hydroxy-2,2,6,6-tetramethylpiperidin-1-oxyl; T_{max}, Maximum temperature of the heat capacity curve (DSC); T_{Onset}, Onset temperature (DSC); UV/VIS, Ultraviolet/Visible light.

* Corresponding author.
E-mail address: karsten.maeder@pharmazie.uni-halle.de (K. Mäder).

https://doi.org/10.1016/j.molliq.2025.127119
Received 30 October 2024; Received in revised form 20 January 2025; Accepted 8 February 2025
Available online 10 February 2025

primarily when oxygen is supplied to bioreactors by sparkling [4].

Amphiphilic molecules are commonly characterised by their nature of surface saturation and self-association properties. A widely used descriptor of concentration-dependent surface activity is the critical micelle concentration (CMC). The CMC describes the concentration of a surfactant in usually aqueous solution at a defined temperature at which the surfaces are almost completely saturated and excess molecules associate in the form of micelles [5]. In addition to sufficient amphiphilicity, the formation of micelles generally requires some flexibility of the molecules. Micelles will not form even at high concentrations if the molecules are too rigid, for example, at lower temperatures [6–8]. Below this critical temperature, surfactant molecules may exist as solid and often crystalline dispersions. Therefore, the critical micelle temperature (CMT) is a second relevant parameter describing the minimal temperature needed for micelle formation at a given surfactant concentration. In the case of commonly used surfactants like polysorbates 20 and 80, the CMT is theoretically below the freezing point and thus below normal formulation temperatures at relevant concentrations [9,10]. Therefore, for convenience, surfactant properties are only described by the concentration of surfactant sufficient to form micelles at a given temperature, i.e. the CMC.

A key factor for micellisation is the ratio of hydrophilic to hydrophobic moieties within the molecule. The ratio of these parts can be expressed by the hydrophilic-lipophilic-balance (HLB). Initially described by Griffin [11], the HLB can range from 0 to 20 for non-ionic surfactants. Amphiphilic molecules with high HLB values (>12) are relatively hydrophilic, whereas those with low HLB values (<8) are more hydrophobic [11–13]. As a result, surfactants with a low HLB tend to exhibit interfacial equilibria, while substances with high HLB values are less surface active. The hydration of the hydrophobic parts of the surfactant by water is thermodynamically unfavourable. Hydrophobic interactions between these groups are preferred when surfactant molecules completely cover the surface [14]. As these interactions lead to the release of free water molecules, micelle formation is thus described as entropy-driven [15,16]. In addition to the HLB, steric effects can hinder micelle formation [17]. It can thus be concluded that all interfaces can be saturated with surfactant; however, micelles will not form if the solubility in water is sufficiently high to make hydrophobic interactions between molecules thermodynamically unfavoured. In addition to these concentration effects, micellisation is highly temperature dependent [14,18,19]. Hydrophobic properties are more pronounced at elevated temperatures because the strength of hydrophilic interdependencies like dipole–dipole interactions decreases at higher temperatures. This leads to a decrease in HLB at higher temperatures, followed by shifts in the equilibrium described earlier. Thus, at higher temperatures, surfaces become saturated earlier, and micelles may form at lower surfactant concentrations.

The transition point from surface saturation to increasing concentration in the solution or micelle formation can be determined in several ways [20]. An indirect approach is to measure the surface tension with increasing surfactant concentration. According to the pseudo-phase separation model, the point at which the surface tension remains constant despite the addition of further surfactant molecules is assumed to represent the CMC [21]. Often, local minima can be observed due to supersaturation, usually caused by small amounts of impurities within the surface-active substance [22,23]. These minima can be used as the point of CMC, while different regression methods are described to determine the CMC when minima are not detectable [21]. However, no statement about the presence of micelles in a solution can be made by surface tension measurements, as a decrease in surface tension would also be observed for amphiphilic molecules that do not form micelles, such as lecithin [24].

A direct method to detect the formation of micelles is using various (fluorescent) dyes [25,26]. When micelles form an additional compartment in solution, hydrophobic dyes, in particular, show increased solubility or partitioning between the micelle core and the surrounding solution. Therefore, UV/VIS measurement can determine the dye solubilisation in micelles. At the same time, suitable fluorescent probes show increased fluorescence intensity and/or a shift in their excitation/emission maxima when partitioned into the more hydrophobic environment. This allows the detection of micelles by both dye solubilisation and fluorescence methods. However, care should be taken when selecting fluorescent probes. Depending on the mechanism underlying the spectral shift, some dyes indicate the simple presence of surfactant without the need for micelle formation. In addition, the dye itself could influence the micelle formation process. To exclude dye-specific artefacts, several dyes should be investigated. Therefore, both Nile Red and Pyrene were used as fluorescent probes for micelles in this study to avoid artefacts and compare different dyes.

Similar to solid-state DSC methods, liquid DSC methods can monitor the differences in heat flow required for the sample and a blank. Therefore, liquid DSC provides insight into molecules' unfolding and refolding processes in solution. Besides determining the thermal protein stability, it also provides insight into micellisation [27–29]. As the term "melting temperature" is misleading in the case of surfactant analysis, the peak maximum temperature (T_{max}) is used. By evaluating T_{max} and T_{Onset}, the minimum temperature for micelle formation at a given concentration can be determined [30]. Therefore, DSC can indicate the critical micelle temperature (CMT) for a given surfactant concentration [31,32].

Dynamic light scattering (DLS) can detect the presence of associated structures, like micelles [33]. In addition to shifts in particle size, the scattered intensity is used as an indication of micelle formation, as larger associations in solution lead to an increase in scattered laser light. A shift in particle size can be observed when the CMC is exceeded. In practice, the method is often limited to relatively high surfactant concentrations (>0.1 $mg{\cdot}mL^{-1}$) compared to dye methods, as a sufficient scattering intensity is required for analysis.

Spectroscopic methods based on magnetic resonance are attractive analytical tools due to their non-invasiveness and specific information content. Both nuclear magnetic resonance (NMR) [34] and electron paramagnetic resonance (EPR) [35,36] have been successfully used to detect micelles. NMR spectroscopy and relaxometry provide insight into the chemical environment of hydrophobic/hydrophilic moieties. Changes in chemical shifts and peak half-height width are associated with micelle formation [37]. CMC determination by EPR is based on the sensitivity of the EPR spectra to the microenvironment. Changes in micro-polarity and micro-viscosity due to micelle formation can be observed due to changes in the spin probes' hyperfine coupling values and rotation correlation times [38–40].

Each CMC/CMT determination method has advantages and disadvantages [20]. CMC determination by surface tension indicates the point of almost complete interface saturation but not directly the formation of micelles. In contrast, dye methods detect the presence of a more hydrophobic compartment without verification of micelle formation. Furthermore, adding mostly hydrophobic dyes or spin probes can alter the system's solubilisation and micelle formation characteristics.

Along with polysorbates 20 and 80, poloxamer 188 (P188) is a stabilising excipient in protein drugs, particularly therapeutic antibodies [4]. Surfactants have been shown to prevent proteins from interacting with the air-water interface, unfolding and forming protein particles. The specific mode of action of each surfactant is under discussion. Three concepts of stabilisation have been proposed: (i) Incorporation of biological agents into micelles, preventing their interaction with surfaces, (ii) saturation of more hydrophobic regions of the protein by surfactant molecules, and (iii) saturation of interfaces by surfactant molecules, preventing interfacial stress on the protein [41]. While (i) protein incorporation into micelles is unlikely, as therapeutic biologics are very similar to or even larger than micelles (e.g. comparing monoclonal antibody drugs formulated with polysorbate 20 or 80), approaches (ii) and (iii) are being investigated in various studies [42]. Researchers have attempted to elucidate the stabilisation mechanism using different

approaches. Comparative measurements of surface tensions with and without protein led to the hypothesis that polysorbates and poloxamers have different mechanisms. Polysorbates are described as preventing unfolding and protein particle formation by saturating interfaces. However, P188 is thought to interact with protein molecules, preventing them from interacting with each other and with solution/ice surfaces [43]. As surface saturation and binding to the protein depend on the concentration and percentage of uncomplexed surfactant, a better understanding of the micellisation behaviour of P188 under pharmaceutical-relevant conditions is beneficial.

As mentioned above, large research efforts have been carried out in recent decades into the micelle formation of poloxamers [2,28,31,44–46], primarily P188. Unfortunately, the existing literature does not give a homogenous picture of the formation of P188 micelles. This can have negative consequences for studies on and with P188. In many cases, micelles are desired or expected; in others, concentrations are chosen to avoid micelles. The aim of this study is, therefore, to compare a variety of methods for the detection of micelles or the determination of the CMC of poloxamer 188 and, by combining the results from these methods, to clarify whether or not micelles below 37 °C should be expected. Here, we gained insight into the behaviour of P188 at the air-water interface by measuring the surface tension using a pendant drop method. By performing liquid DSC experiments on P188 solutions, we determined a temperature range in which the endothermic unfolding processes of P188 molecules occur. In addition, we observed the formation of a hydrophobic compartment using fluorescent probes and detected their partitioning between the micro-compartment and the surrounding solution. Nile Red and Pyrene were used as fluorescent dyes to monitor changes in the P188 solutions. We decided to use Tempolbenzoate as a hydrophobic spin probe in EPR experiments to characterise the micro-viscosity and micro-polarity of P188 solutions as a function of the P188 concentration and temperature. Furthermore, we decided to use NMR spectroscopy to get additional information on the behaviour and chemical environment of the P188 molecules.

2. Experimental

2.1. Materials

All samples were prepared using fresh Milli-Q-grade water. Poloxamer 188 (Poloxamer 188 PRO; batch no. SLCM7013; 82.1 % content of oxyethylene moieties and a relative molecular mass of 8599) was purchased by Sigma-Aldrich Chemie GmbH, Taufkirchen, Germany, and was used as received for all analyses. Trisodium citrate dihydrate (Fisher Scientific UK, Loughborough, United Kingdom); citric acid monohydrate (Jungbrunzlauer Ladenburg GmbH, Ladenburg, Germany); sodium chloride (Honeywell International, Inc., Morris Plains, NJ, USA); trehalose dihydrate (Pfanstiel, Inc., Waukegan, IL, USA); Tempolbenzoate (4-hydroxy-2,2,6,6-tetramethylpiperidin-1-oxylbenzoate; Sigma-Aldrich Chemie GmbH, Taufkirchen, Germany); Nile Red (9-(Diethylamino)-5H-benzo[a]-phenoxazin-5-on; Tokyo Chemical Industry Co., LDT., Tokyo, Japan); Pyrene (Tokyo Chemical Industry Co., LDT., Tokyo, Japan); methanol (Merck KGaA, Darmstadt, Germany) and deuterium oxide (Sigma-Aldrich Chemie GmbH, Taufkirchen, Germany) were used as received.

3. Methods

3.1. Sample preparation

P188 and all buffer substances were dissolved in Milli-Q water with stirring at room temperature. To prepare a dilution series, both the concentrated P188 stock solution (up to 200 mg·mL^{-1}) and the corresponding pure buffer solution were filtered through a 0.22 μm PVDF (polyvinylidene fluoride) syringe filter (Carl Roth GmbH + Co. KG; Karlsruhe, Germany) before stepwise dilution. Dilution was performed by pipetting surfactant solution to pure solvent at a ratio of 1 to 1 or 1.5 to 1, starting from 160 mg·mL^{-1}. P188 solutions were mixed by pipetting before the next dilution step. If not measured immediately, all solutions were stored at 5 °C and used within 24 h. The characteristics of P188 in five buffer systems were investigated. The used abbreviations for those systems and their composition are explained in Table 1.

3.2. Differential Scanning Calorimetry (DSC)

Differential scanning calorimetry measurements of P188 solutions were performed using a MicroCal PEAQ-DSC Automated (Malvern Panalytical Ltd, Malvern, United Kingdom). After preparation, samples were stored in covered 96-well plates (Malvern Panalytical Ltd, Malvern, United Kingdom) in the thermostatically controlled autosampler at 8 °C. Samples were scanned from 5 °C to 105 °C at a heating rate of 1.5 K per minute. Analysis was performed in duplicate. Raw data analysis was performed using MicroCal PeaQ-DSC software (Malvern Panalytical Ltd, Malvern, United Kingdom). The heating rate curve of the pure buffer was subtracted from the sample curves, and the baseline was manually adjusted. T_{max} and T_{Onset} were evaluated using MicroCal PeaQ-DSC software (Malvern Panalytical Ltd, Malvern, United Kingdom). Raw data and peak analysis results were exported and used for graphical presentation.

3.3. Dynamic Light Scattering (DLS)

A Prometheus Panta (NanoTemper Technologies, Inc., South San Francisco, CA, USA) was used to determine the particle size in solutions. The samples were filled into high sensitivity capillaries (Prod. No. PR-C006; NanoTemper Technologies, Inc., South San Francisco, CA, USA) and measured using the Panta Control software (NanoTemper Technologies, Inc., South San Francisco, CA, USA) in the size determination mode. Properties were set to high sensitivity (10 measurements, 5 s) and 100 % laser power for all samples. The temperature was controlled by the instrument, and measurements were performed in ascending temperature order. The data was analysed using Panta Analysis software (NanoTemper Technologies, Inc., South San Francisco, CA, USA). Size distribution data were exported and used for the graphical visualisation.

3.4. Fluorescence dye methods

A FluoroMax 4 spectrometer (HORIBA Europe GmbH, Oberursel, Germany) controlled by FluorEssence software (HORIBA Europe GmbH, Oberursel, Germany) was used for the fluorescence measurements. 2.5 mL samples were filled into disposable fluorescence cuvettes (Carl Roth GmbH + Co. KG; Karlsruhe, Germany) and tempered to the desired temperature using a TC-1 temperature controller (Quantum Northwest, Inc., Liberty Lake, WA, USA) with a tempered cuvette holder. The samples were equilibrated for 1 min per °C temperature change.

3.4.1. Pyrene

Samples were prepared by adding 10 μL of a 0.25 mM methanolic Pyrene solution to glass containers and evaporating the solvent to complete dryness. The containers were filled with 5 mL of the P188

Table 1
Abbreviations and composition of the investigated buffer systems.

Abbreviation	Composition of solvent
W	Pure **W**ater
CSC	**C**itrate buffer (pH 6.0, 25 mM), 115 mM **S**odium **C**hloride
CSCT200	**C**itrate buffer (pH 6.0, 25 mM), 115 mM **S**odium **C**hloride, **200** mM **T**rehalose
CSCT400	**C**itrate buffer (pH 6.0, 25 mM), 115 mM **S**odium **C**hloride, **400** mM **T**rehalose
CSCT800	**C**itrate buffer (pH 6.0, 25 mM), 115 mM **S**odium **C**hloride, **800** mM **T**rehalose

solutions with defined surfactant concentrations and were sonicated for 30 min to obtain samples containing 0.5 μM Pyrene. Fluorescence spectra were recorded between 350 nm and 500 nm with an excitation wavelength of 336 nm. The ratio of the maximum fluorescence intensities between 370–374 nm and 390–394 nm was calculated and used for the graphical illustration.

3.4.2. Nile Red

A 1 mM stock solution of Nile Red in methanol was prepared. 25 μL of the stock solution was dissolved in 9.98 mL of the appropriate solvent. A volume of 0.5 mL of these solutions was mixed with the surfactant solutions to obtain samples with specific surfactant concentrations and 0.5 μM Nile Red. Fluorescence spectra were recorded between 580 nm and 780 nm with an excitation wavelength of 550 nm. The ratio of the fluorescence intensity at 626 nm and 656 nm emission wavelength was calculated and used for graphical representation.

3.5. Drop Shape Analysis (DSA)

A pendant drop method was used to determine the surface tension using a DSA25E (KRÜSS GmbH, Hamburg, Germany) in combination with a DC-11 heating chamber (KRÜSS GmbH, Hamburg, Germany). ADVANCE software (KRÜSS GmbH, Hamburg, Germany) was used to control the device, perform the measurements and calculate the surface tension. The chamber temperature was controlled by a CORIO CD-200F circulation thermostat (JULABO GmbH, Seelbach, Germany), and a digital thermometer monitored the temperature in the chamber. A Petri dish filled with the appropriate buffer was placed in the chamber to prevent excessive evaporation of water from the droplet. A glass syringe with a Teflon-coated needle (1 mm diameter) was used for the droplet formation. The solutions were tempered to the desired temperature in a water bath for at least 10 min before analysis. The drop volumes were set to approx. 90 % of the volume that caused the drop to fall during the measurement procedure. Three images of each droplet were taken immediately after the formation of the droplet and after 30 s, 60 s, and 90 s of droplet lifetime. The average of the three images was calculated. This procedure was repeated three times for each sample. For better comparison, the relative surface tension was calculated by subtracting the pure buffer value. The graphs show the mean and the standard deviation of the three series of measurements for each sample after 90 s of droplet lifetime.

3.6. Electron Paramagnetic Resonance Spectroscopy (EPR)

A 250 mM methanolic Tempolbenzoate solution was spiked to the samples to give a Tempolbenzoate concentration of 1 mM. The samples were mixed and sonicated for 15 min before being filtrated through a 0.22 μm polyvinylidene difluoride syringe filter (Carl Roth GmbH + Co. KG; Karlsruhe, Germany). 10–15 μL of these sample solutions were filled into micropipettes (BLAUBRAND® intraMARK, Wertheim, Germany), capped with capillary tube sealant (CRITOSEAL®, Leica Microsystems, Wetzlar, Germany) and inserted into the spectrometer, respectively. Continuous wave electron paramagnetic resonance spectroscopy was performed using a Miniscope MS 5000 (Magnettech GmbH, Berlin, and Freiberg Instruments, Freiberg, Germany). The instrument was controlled by the appropriate Freiberg Instruments software, and the temperature was controlled using an MS 5000 (Magnettech GmbH, Berlin, Germany). The controller was set to the desired temperature, and the sample was equilibrated for 5 min. All measurements were performed in the X-band range with a magnetic field sweep of 8 mT centred around 337.6 mT. The scan time was 60 s, the modulation amplitude (100 kHz) was set to 0.05 mT, and a microwave power of 5 mW was chosen for the measurement. Each spectrum is an accumulation of 5 successive scans. After the measurement, the sample was heated to the next higher temperature step. The EasySpin program [47] running on Matlab software (The MathWorks, Inc., Natick, MA, USA) was used to evaluate the rotation correlation time τ_c and the hyperfine splitting value A_N. All spectra were baseline corrected and fitted for τ_c with the "garlic" function. A_N was calculated from the peak positions of the first and third maxima.

3.7. Nuclear Magnetic Resonance Spectroscopy (NMR)

NMR data were acquired on a BRUKER Avance III spectrometer (Bruker Corporation, Billerica, MA, USA) operating at a frequency of 800.23 MHz for proton and 200 MHz for carbon, respectively, with a cryogenically cooled TXO probe head (Bruker Corporation, Billerica, MA, USA) optimised for ^{13}C- NMR. Standard BRUKER library pulse sequences were used for data acquisition. Sample temperature was controlled by a calibrated (±0.5 °C) BVST unit (Bruker Corporation, Billerica, MA, USA). Chemical shift reference values were obtained using a second sample with DSS (sodium trimethylsilylpropanesulfonate) for proton and carbon referencing. Raw data was evaluated using MestReNova Version 15.0.1–35756 (Mestrelab Research S.L., Santiago de Compostela, Spain). Spectra were processed by phase correction (Auto Phase Correction), baseline correction (Auto Baseline Correction, Full Auto (SNP)) and denoising ('Non-local Means' method, 0.500 noise factor and 'Blockwise' mode). Spectra were normalised by setting the highest intensity to 100 %. Peaks were analysed using the Auto Peak Picking function (GSD method, positive peaks only, refinement level: 3 (10 fitting cycles)). Spectra and peak properties (chemical shift and half-height width) were exported and used for graphical evaluation.

4. Results and discussion

The micelle formation behaviour of surfactants is often more complex than described in theory [48,49]. On one hand, the distribution of the surfactant molecules occurs not only between the interface and the solution but also between the monomolecular and the micellar state. On the other hand, the formation of different molecular conformations at the interface leads to the complexity of the surface saturation. In addition, a pronounced temperature dependence on the hydrophilicity of surfactants leads to significant shifts in the CMC at different temperatures. Furthermore, surfactants are composed of different compounds with different properties. Different surfactant molecules can have different interfacial and micelle formation tendencies. A critical micelle concentration range (CMCR) has been proposed instead of a single CMC value [48]. The CMCR groups the individual CMCs of multicomponent surfactants as a range where micellisation probably occurs. The CMC and CMT evaluation methods examine very different properties of surfactant solutions. Therefore, the values obtained may differ, especially when micellisation is more complex. Dye methods tend to indicate micellisation as soon as the first micelles are present in the solution, whereas the surface tension may not be constant at this concentration. In this study, we performed a series of experiments using different analytical methods on a single batch to get a comprehensive overview of the micelle formation behaviour of P188.

4.1. Differential Scanning Calorimetry (DSC)

The behaviour of P188 in solution was characterised as a function of temperature using liquid differential scanning calorimetry (DSC). Poloxamers are known to display the capacity to undergo the rearrangement of individual molecules within a solution. It is postulated that intramolecular complexes in the form of flat rings of single poloxamer molecules are formed [1,3]. Under these circumstances, the PEO chains enclose the PPO moiety, facilitating more effective interaction with the surrounding water. Upon reaching the T_{Onset}, the intermolecular interactions between PPO and PEO chains begin to collapse under energy absorption, resulting in an endothermic event observed in the DSC analysis [2,28,50]. Given that these non-complex P188 molecules are a prerequisite for micelle formation, the DSC data can provide valuable

insights into the minimum temperature required for micelle formation. T_{max} and T_{Onset} are therefore used as indicators of the critical micelle temperature (CMT). The relationship between the unfolding processes and the formation of micelles has been previously postulated in the literature [31,51,52]. The presence of further solutes may influence the unfolding of poloxamer molecules, consequently affecting the process of micelle formation. Fig. 1 shows the outcomes of the T_{max} assessment of 10 mg·mL^{-1} P188 in water in the presence of different solutes. The impact of ammonium sulphate, sodium chloride, and guanidine hydrochloride on the maximum peak temperature (T_{max}) can be seen. In comparison to pure water, the addition of 1 M sodium chloride leads to a decrease in T_{max} by 16.9 K, while the presence of 0.5 M ammonium sulphate leads to a further reduction of T_{max} by up to 24.8 K. On the other hand, adding 1 M guanidine to the solution resulted in a 4.8 K increase in T_{max} relative to the control sample (pure water).

The hydrophilicity of the polyethylene oxide (PEO) segment is highly temperature dependent. Dipole interactions between water and the poloxamer are averaged out by the increased mobility of the molecules with increasing temperature. This results in the poloxamer becoming more hydrophobic, thereby increasing its affinity for surfaces and the formation of micelles. This temperature effect also affects the solubility of proteins and polymers. In particular, salts can exert a significant influence on the water cluster. The disruption of the water cluster by chaotropic substances, such as guanidinium, increases the number of "unsaturated" hydrogen bonds. This effect can be exploited by attenuating the hydrophobic effect of proteins or polymers in solution to enhance the solubility of proteins, otherwise known as salting-in. Conversely, anti-chaotropic (or kosmotropic) substances such as ammonium sulphate augment the hydrophobic effect by reinforcing the interactions between water molecules, thereby reducing solubility (the "salt-out" effect).

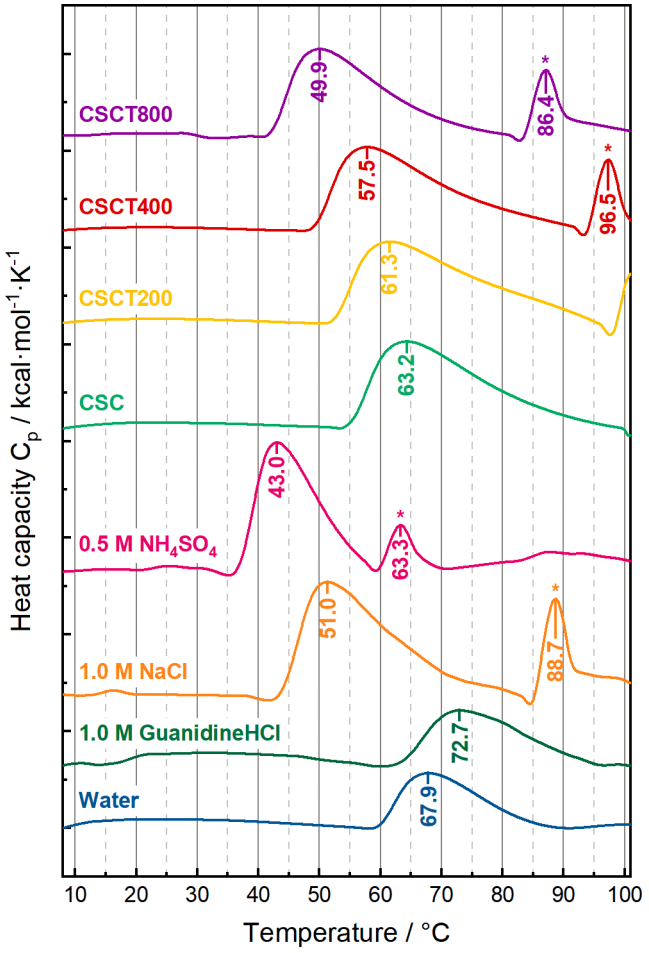

Fig. 1. Heat capacity (C_p) curves (heating rate: 1.5 K·min^{-1}) of 10 mg·mL^{-1} P188 in all investigated aqueous systems. C_p was calculated against the pure solvent with a theoretical molar mass for P188 of 8'600 Da. The first endothermal event is attributed to the unfolding process of P188 molecules during micelle formation. Additional endothermic processes are assigned to reaching the cloud point and marked with a star.

The affinity of P188 to the interface and its micellisation behaviour may be influenced by buffer substances and tonicity agents, depending on the nature of the solute and its concentration [53]. Similar effects are described for poloxamer 407 [32] and other poloxamers [28,54]. The impact of anti-chaotropic salts (ammonium sulphate > sodium chloride) and chaotropic-acting guanidinium on P188, in comparison to pure water, is evident in the alterations of T_{max}. The presumed impact of these solutes on the transition temperature of P188 in solution is demonstrated, aligning with the principles of the Hofmeister series and the findings of Alexandridis et al. (1997) [28]. Moreover, the hydrophobicity of the polymers can be augmented until the cloud point of the surfactant is reached. This phenomenon has also been demonstrated for other relatively hydrophilic poloxamers in the presence of salts [54,55]. The results from DSC measurement show additional endothermic events at temperatures above the first unfolding/micellisation peak (see Fig. 1). These signals can be attributed to the attainment of the cloud point.

Subsequently, studies were conducted on P188 in buffer systems that are more pertinent to pharmaceutical formulations. Besides solutions of P188 in pure water, samples in 25 mM citrate buffer (pH 6) containing 115 mM NaCl were investigated, and the samples in which 200 mM, 400 mM, and 800 mM trehalose were added to this buffer system. The abbreviations for these aqueous systems are in the Methods sections (Table 1). The results of T_{max} and T_{Onset} determination are illustrated in Fig. 2. The linear regression of the semi-logarithmic plot demonstrates the logarithmic correlation between the concentration of P188 and T_{max}/T_{Onset}. The relationship is expressed by Equation 1. The results of the linear regression of the data points are presented in Table 2.

Equation 1: Linear regression equation for T_{max} and T_{Onset} values

$$Temperature = \ln Concentration\,P188 * Slope + Intercept$$

Similar to sodium chloride, ammonium sulphate or guanidine, the addition of citrate buffer, sodium chloride, and trehalose showed a significant shift in T_{max} and T_{Onset}. Fig. 1 illustrates the DSC curves for all buffer systems and 10 mg·mL^{-1} P188. The exchange of pure water by citrate buffer containing 115 mM sodium chloride as solvent led to a negative shift in temperature values of approx. 5 K. Adding a further 200 mM trehalose resulted in a further decrease of 2.6 K, giving a total decrease of −7.6 K in contrast to water. An increase in trehalose concentration to 400 mM resulted in a total shift of approximately 12 K, while 800 mM trehalose produced an almost 20 K reduction in T_{max}/T_{Onset} relative to water.

It can thus be concluded that citrate buffers, including sodium chloride, exert a kosmotropic effect on the water cluster. These observations regarding trehalose are in accordance with the findings of previous studies on disaccharide-water mixtures [56]. Adding trehalose as a solute increases the hydrophobic effect of P188 in solution and lowers the temperature required to reduce the hydrophilic interactions between P188 molecules and water. Therefore, the unfolding process of P188 and the assembly of PPO fractions of several P188 molecules in the form of a micelle core occurs at lowered temperatures. Adding 25 mM citrate buffer and 115 mM sodium chloride to water reduces the critical micelle temperature (CMT) of P188 by 5 K. Moreover, our data demonstrate a linear correlation between the critical micelle temperature (CMT) and the logarithm of the P188 concentration (Fig. 2, Table 2). Therefore, the relative impact on temperatures is more pronounced in the low concentration range and diminishes at high concentrations.

The linear regression data obtained from the semilogarithmic plot can be used to calculate the P188 concentrations required to reach a

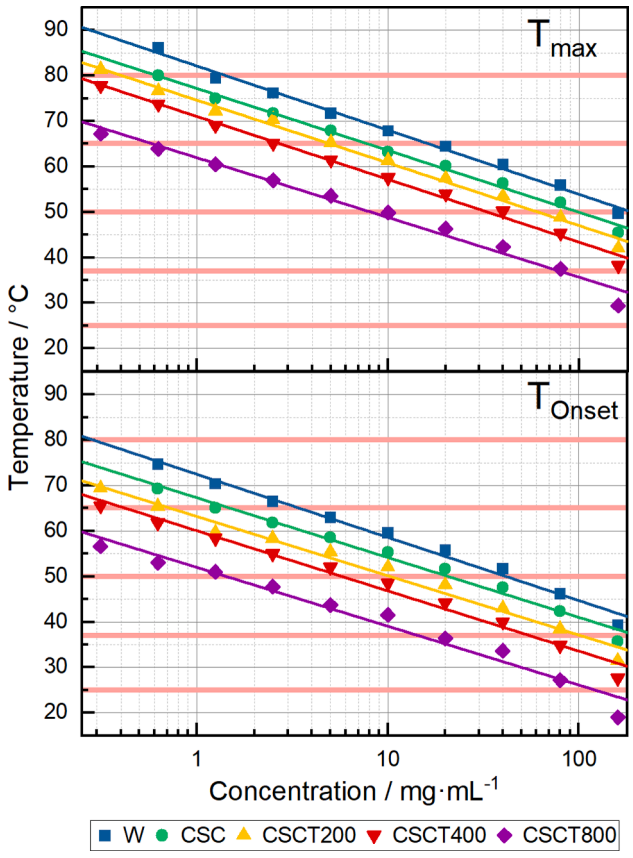

Fig. 2. Peak maximum temperature (T_{max}) and peak onset temperature (T_{Onset}) derived from the heat capacity curve obtained by DSC (Differential Scanning Calorimetry) for all buffers and P188 concentrations between 0.3125 mg·mL^{-1} and 160 mg·mL^{-1}. A logarithmical scale is used for the x-axis. Water (W; Blue squares), 25 mM citrate buffer with 115 mM sodium chloride (CSC; Green circles), 25 mM citrate buffer with 115 mM sodium chloride and 200 mM trehalose (CSCT200; yellow upright triangles), 25 mM citrate buffer with 115 mM sodium chloride and 400 mM trehalose (CSCT400; Red inverted triangles) and 25 mM citrate buffer with 115 mM sodium chloride and 800 mM trehalose (CSCT800; purple diamonds) are shown. Curves of 0.3125 mg·mL^{-1} P188 in water (W) and 25 mM citrate buffer + 115 mM sodium chloride were not evaluable due to a low signal-to-noise ratio. Linear regression lines described in Table 2 are shown in the graphs. Temperatures tested in other experiments are highlighted in light red.

Table 2
Linear regression data for peak maximum (T_{max}) and onset (T_{Onset}) temperatures according to Equation 1.

Sample	T_{max}/°C			T_{Onset}/°C		
	Intercept	Slope	Adj. R-Square	Intercept	Slope	Adj. R-Square
W	82.08	−14.11	0.993	72.45	−13.88	0.986
CSC	77.11	−13.6	0.994	67.29	−13.15	0.984
CSCT200	74.54	−13.78	0.992	63.17	−13.03	0.979
CSCT400	70.96	−13.81	0.993	60.03	−13.23	0.982
CSCT800	61.9	−13.13	0.982	51.97	−12.93	0.964

specified T_{Onset} or T_{max}. The calculated data for the temperatures under investigation are presented in Table 3.

As temperature increases, the concentration required to demonstrate endothermal processes decreases. To shift T_{Onset} and T_{max} to temperatures of 15 °C or below, a concentration of P188 more than 160 mg·mL^{-1} is required in all buffer systems. In CSCT800, the theoretically (calculated) concentration needed to reduce T_{Onset} to 25 °C is 121.9 mg·mL^{-1}, implying that micelle formation has begun but may not be complete, given that T_{max} is above 25 °C. When T_{Onset} is (theoretically) set to 37 °C, the calculated concentration for all trehalose-containing samples is below 160 mg·mL^{-1}. It is only in CSCT800 that a T_{max} of 37 °C is feasible at 78.8 mg·mL^{-1}, thus within the evaluated concentration ranges. T_{max} is predicted to be potentially reached at 50 °C in all buffers with concentrations below 160 mg·mL^{-1}, except for water. It is possible to achieve T_{Onset} and T_{max} values of 65 °C and 80 °C in all tested buffer systems within a P188 concentration range of <160 mg·mL^{-1}. This indicates that the CMC for P188 is below 160 mg·mL^{-1} at these temperatures. It should be noted that values that fall outside the calibration curve, as calculated from the regression data, may be subject to error, given that these concentrations were not within the scope of this study.

The DSC measurements demonstrated a CMT-lowering effect of citrate buffer with sodium chloride and trehalose as solutes in aqueous P188 solutions. It can be assumed that micellisation occurs when T_{max} is reached. Consequently, no micelle formation is expected at 25 °C for any buffer system with P188 concentrations below 160 mg·mL^{-1}.

4.2. *Particle Size Determination by Dynamic Light Scattering (DLS)*

Dynamic light scattering can be employed to detect micelle formation, as evidenced by an increase in scattering intensity and particle size at CMC/CMT. While the scattering intensity and the signal-to-noise ratio are essential for valid data evaluation, only concentrations exceeding 0.625 mg·mL^{-1} were measured and plotted. Intensity-weighted size distributions for samples in CSCT200 are exemplified in Fig. 3.

A notable alteration in particle size can be discerned when the temperature exceeds a solvent- and concentration-specific threshold. In the case of CSCT200, only particle diameters below 10 nm were observed at temperatures of 15 °C, 25 °C and 37 °C. Attaining a temperature of 50 °C results in a discernible shift in the intensity-weighted particle size. At this temperature, the intensities are found to be highly similar at both 25 °C and 37 °C for a concentration range of 0.625 mg·mL^{-1} to approximately 30 mg·mL^{-1}. At elevated concentrations, the intensity-weighted particle diameter increases to approximately 15 nm. This trend persists at elevated temperatures, precisely 65 °C and 80 °C. At 65 °C, high intensities of particles, approximately 15 nm in size, are observed at concentrations above 2.5 mg·mL^{-1}. Conversely, particles of this size can be detected for all measured concentrations at 80 °C (≥0.625 mg·mL^{-1}). Notably, in addition to a change in particle diameter, there is an increase in intensity during the formation of larger assemblies.

The size distribution data of all the investigated buffer systems at six different temperatures are presented in Fig. 4 and Fig. 5. As previously outlined by Zhou et al. (1988) in their DLS studies, the diameter range for premicellar particles should be below 5 nm (illustrated in light blue), while micelles are anticipated to have diameters of approximately 15 nm [33]. The interval between these extremes can be defined as a transition zone in which both premicellar and micellar structures may be found.

The water (W) and citrate buffer plus sodium chloride (CSC) systems exhibit single-intensity peaks in the 5 nm range between 15 °C and 37 °C (Fig. 4). At 50 °C, the formation of shoulders or multi-peaks is observed. It can be postulated that this initial shift in particle diameter represents the transition zone between monomers and micelles, as previously described. At 50 °C, this behaviour is more pronounced in CSC than in W, which suggests that the transition from monomers to micelles may be more advanced in CSC than in pure water. At 65 °C, a discernible shift in the peaks towards the 15 nm range is observable. Samples of water with a concentration of P188 above 10 mg·mL^{-1} exhibited a shift towards 15 nm, while a concentration of 10 mg·mL^{-1} P188 demonstrated an initial change in the size distribution. In CSC buffer, this phenomenon occurs for P188 concentrations ranging from 2.5 mg·mL^{-1} to 5 mg·mL^{-1}. However, solutions with concentrations exceeding 10 mg·mL^{-1} exhibit a shift towards higher diameters. The results demonstrate that the

Table 3
Calculated P188 concentrations for defined DSC peak event maximum and onset temperatures using Equation 1. Values <0.3125 mg·mL^{-1} and >160 mg·mL^{-1} are out of the linear regression range.

	W		CSC		CSCT200		CSCT400		CSCT800	
Temp. / °C	T_{Onset}/ mg·mL^{-1}	T_{max} / mg·mL^{-1}	T_{Onset} / mg·mL^{-1}	T_{max} / mg·mL^{-1}	T_{Onset} / mg·mL^{-1}	T_{max} / mg·mL^{-1}	T_{Onset} / mg·mL^{-1}	T_{max} / mg·mL^{-1}	T_{Onset} / mg·mL^{-1}	T_{max} / mg·mL^{-1}
5	>160.0	>160.0	>160.0	>160.0	>160.0	>160.0	>160.0	>160.0	>160.0	>160.0
15	>160.0	>160.0	>160.0	>160.0	>160.0	>160.0	>160.0	>160.0	>160.0	>160.0
25	>160.0	>160.0	>160.0	>160.0	>160.0	>160.0	>160.0	>160.0	121.9	>160.0
37	>160.0	>160.0	>160.0	>160.0	101.9	>160.0	55.06	>160.0	14.39	78.78
50	41.41	>160.0	20.65	98.38	10.25	60.38	5.731	32.95	1.421	8.057
65	3.44	16.24	1.493	7.766	0.7236	4.923	0.4212	2.702	<0.3125	0.5801
80	<0.3125	1.404	<0.3125	0.613	<0.3125	0.4013	<0.3125	<0.3125	<0.3125	<0.3125

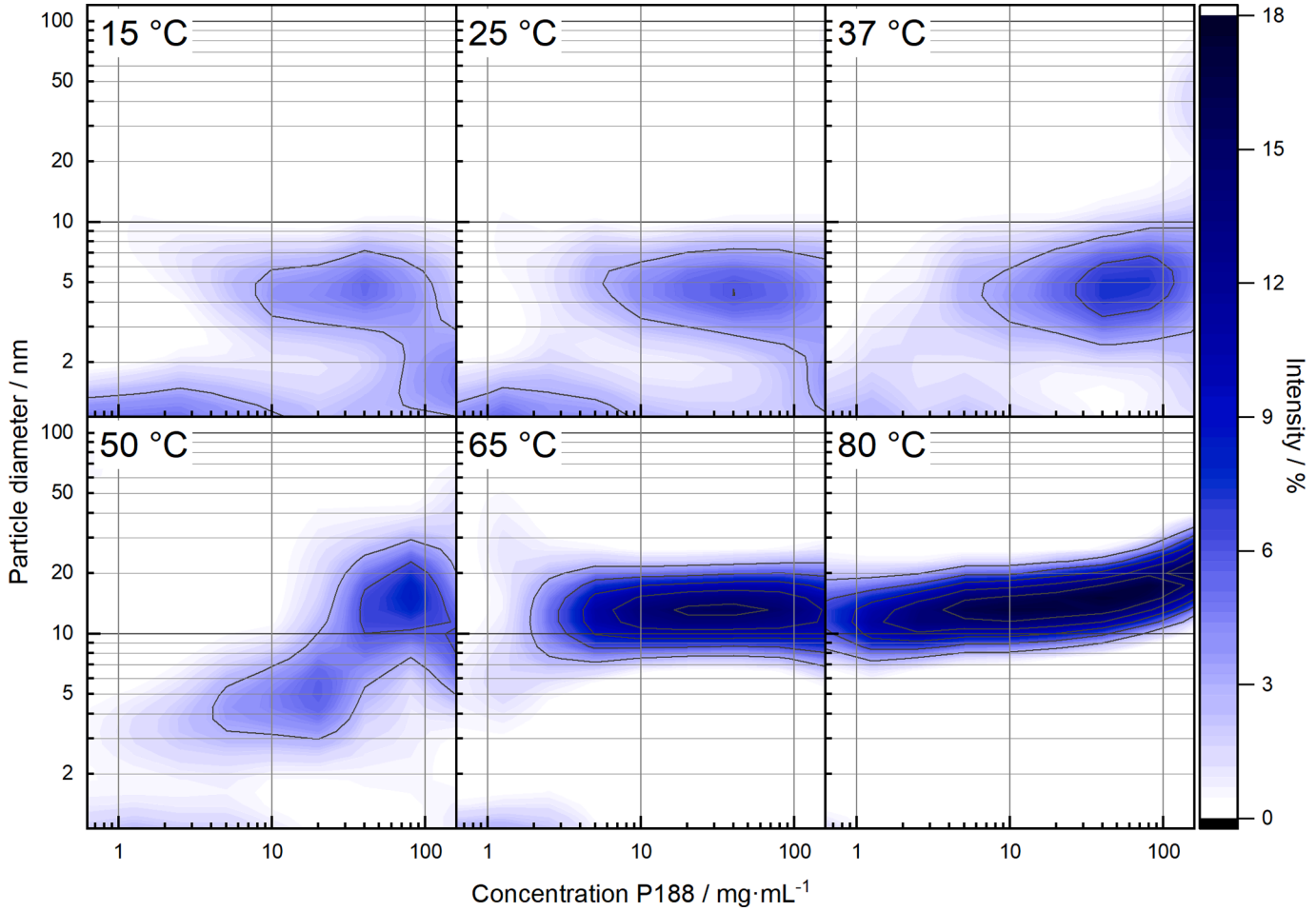

Fig. 3. Results of dynamic light scattering (DLS) measurements: Section of intensity weighted size distributions for P188 samples in CSCT200 buffer. Diameter from 1 nm to 120 nm and concentrations from 0.625 mg·mL^{-1} to 160 mg·mL^{-1} are shown. Areas of high signal intensities are coloured more intense blue.

transition from single molecules into micelles occurs at lower temperatures in CSC than in W. At 80 °C, both W and CSC buffer exhibit a single peak with increased intensity in the 15 nm range for all tested concentrations, suggesting the formation of micelles in all investigated P188 concentrations.

The incorporation of trehalose into CSC results in a concentration-dependent generation of scattering signals within the range of <2 nm (Fig. 5). As previously described for the disaccharide sucrose [57], light scattering by the trehalose molecule is likely to occur within approximately 1 nm. The signals mentioned above are more pronounced at low concentrations of P188. This can be explained by the superimposition of the trehalose signal by the P188 scattering, given that smaller particle sizes exhibit exponentially lower light scattering. In the case of CSCT200, peaks in the 5 nm range are observed when the concentration of P188 exceeds 2.5 mg·mL^{-1}. In CSCT400, the contrast of a peak in the 5 nm region requires higher concentrations, precisely 10 mg·mL^{-1} and above. In CSCT800, no sufficient signal could be identified within the 5 nm range, irrespective of temperature or concentration. At the temperature at which a shift in peaks can be observed, peaks in the 15 nm region occur with high maximum intensities. CSCT200 exemplifies this phenomenon at 50 °C, wherein concentrations exceeding 40 mg·mL^{-1} manifest the abovementioned shift. In CSCT400 at 50 °C, concentrations above 20 mg·mL^{-1} are sufficient to form particles in the 15 nm range, with a nascent change observable at 37 °C for both highest concentrations. As previously outlined, the intensity of light scattering is markedly influenced by particle size. Given that the dimensions of disaccharides

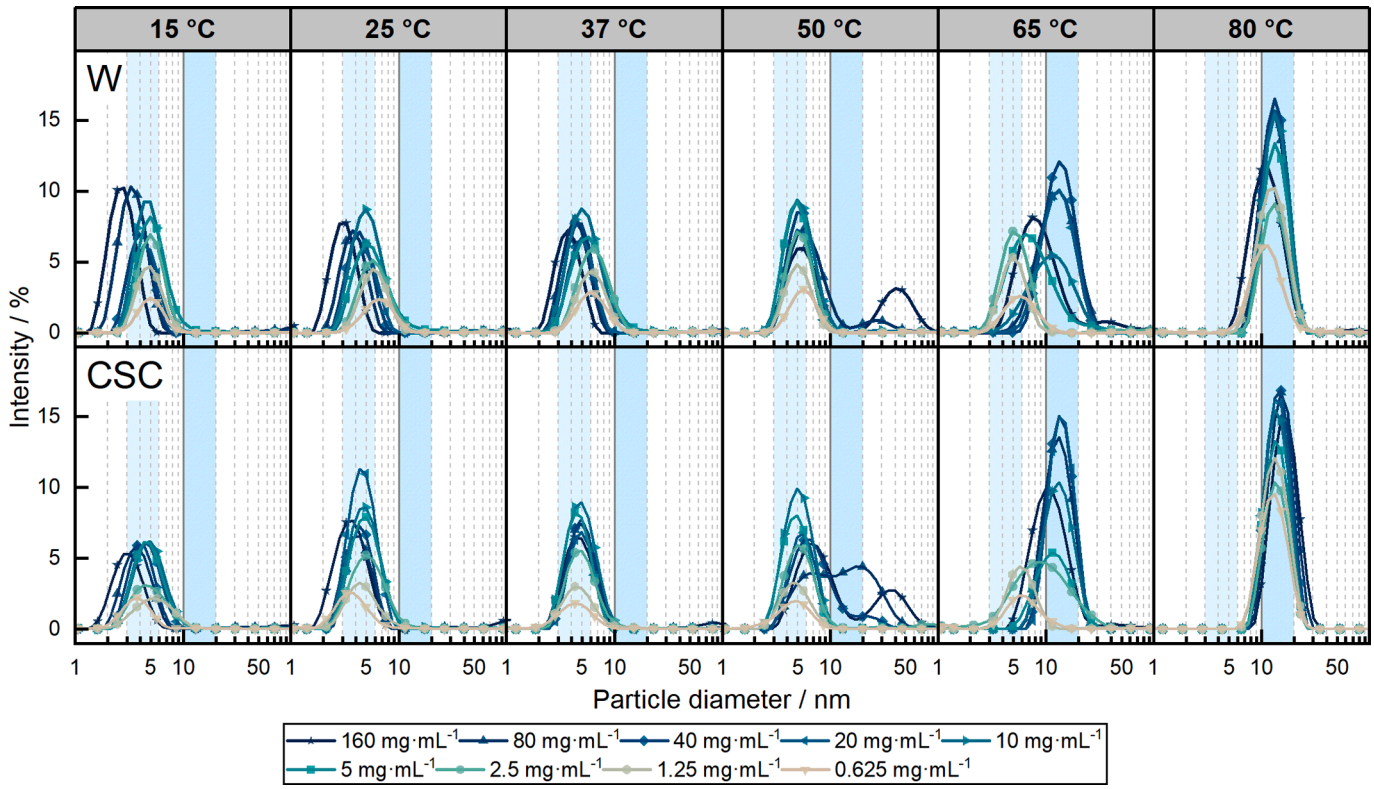

Fig. 4. Intensity-weighted size distribution data for P188 in water (W) and citrate buffer (CSC). P188 concentrations from 0.625 mg·mL^{-1} to 160 mg·mL^{-1} are shown. Particle diameters of interest (3–6 nm and 10–20 nm) are highlighted and discussed in this chapter.

fall within the range of 1 nm, these particles exhibit minimal light scattering intensity. A similar effect can be observed in pre-micellar structures with a diameter of approximately 5 nm. At the point of transition from these monomers to micelles with a diameter of 15 nm, there is a notable increase in the scattering intensity. Therefore, peaks in the 15 nm range may be more likely to emerge than to shift from smaller particle diameters if these do not show sufficient scattering intensity.

It is hypothesised that P188 forms intramolecular associates, which can account for particle diameter in a range of 5 nm when either P188 concentration or temperature is insufficient to induce micelle formation. Upon reaching the CMT, particles in the range of 15 nm are formed. The attainment of an almost constant level of size in the range of 15 nm signifies the conclusion of the transition phase from premicellar structures to micelles. This diameter is consistent with the data presented in the literature regarding the sizes of P188 micelles [33]. Therefore, the alteration in particle size during a temperature increase indicates the formation of micelles and the point of CMT.

Given that the CMC is temperature-dependent, a reduction in the concentration of P188 will result in a shift in size at higher temperatures. Conversely, a decrease in temperature results in a change if the concentration of P188 is increased. Increased temperature results in a reduction in hydrophilic interactions between water molecules and the PEO/PPO moieties. The P188 molecule becomes more hydrophobic, thereby increasing the number of molecules available for intermolecular interactions, which in turn leads to the formation of micelles. An increase in concentration results in a greater absolute number of molecules undergoing micellisation, necessitating lower temperatures to induce micelle formation.

The point of shift in particle size also depends on the presence of solutes in the solution. Consistent with the results from DSC, citrate buffer decreases the CMC/CMT in contrast to pure water. Adding trehalose to the citrate buffer leads to a further decrease in temperature/concentration needed for micelle formation, indicated by a shift in size from the 5 nm to the 15 nm range. At the same time, this effect scales with the amount of trehalose added. These findings agree with DSC data and support the idea of the lack of P188 micellisation below 37 °C, especially investigated by Alexandridis et al. (1994) [2,45].

For illustrative purposes, the results of DLS are presented as intensity-weighted size distributions, as calculations of an average particle size (e.g. Z-average) from multimodal distributions are not a reasonable approach and are susceptible to error. Furthermore, it is essential to acknowledge that the accuracy of size measurements obtained by DLS is contingent upon several variables. Firstly, it is crucial to have precise knowledge of the solution viscosity, which affects the Brownian motion. Viscosity itself is influenced by a few factors, including temperature, the presence of solutes and their concentrations. The viscosity of P188 solutions displays a more intricate response to temperature fluctuations than that observed in pure solvents. In particular, high concentrations of P188 may result in a notable increase in viscosity due to the tendency of poloxamers to form thermo-reversible gels [58]. This may be the reason for the slight shift in the intensity of peaks in the 400 mM and 800 mM trehalose samples at 80 °C. The elevated viscosity of the solution in question is responsible for the larger particle size observed in the DLS calculation. The device software calculates the viscosity data under the assumption of a simple temperature-viscosity relation. Consequently, the particle diameters for high-concentrated P188 solutions are susceptible to being calculated with a degree of inaccuracy. However, this study aimed to investigate particle size shifts rather than provide precise size measurements.

These observations were made in the context of a series of experiments conducted at varying temperatures to determine the effect of temperature on the shifts mentioned above. As the temperature increased, the concentration of P188 at which this shift occurred decreased. The observed increase in particle size can be attributed to the unfolding of coiled P188 molecules and the subsequent formation of micelles. In addition to the temperature-dependent behaviour, introducing solutes, specifically citrate buffer, sodium chloride and trehalose, reduces the P188 concentration at which micelles are formed.

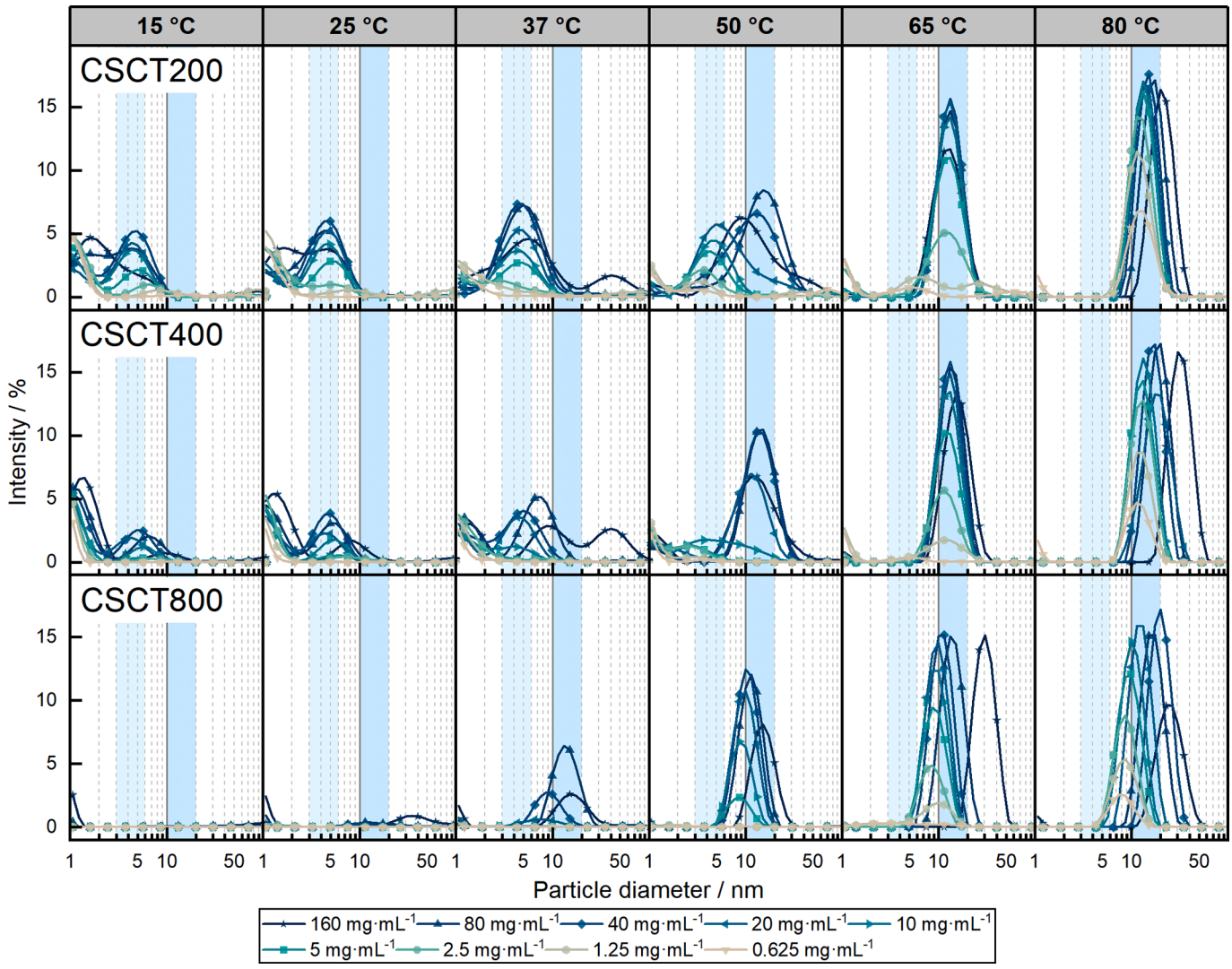

Fig. 5. Intensity-weighted size distribution data for P188 in citrate buffer plus sodium chloride containing 200 mM (CSCT200), 400 mM (CSCT400), and 800 mM trehalose (CSCT800). P188 concentrations from 0.625 mg·mL^{-1} to 160 mg·mL^{-1} are shown. Particle diameters of interest (3–6 nm and 10–20 nm) are highlighted and discussed in this chapter.

4.3. Dye methods

4.3.1. Alterations in Nile Red fluorescence spectra during micellisation

The fluorescence spectra of 0.5 μM Nile Red in the sample solutions were obtained. The excitation wavelength of 550 nm revealed that the emission maximum was 656 nm in the surfactant-free samples and 626 nm in the case of micellar poloxamer solutions. These wavelengths are in line with the literature [59,60] and were found to be independent of the presence of solutes. As the absolute intensity is dependent on the concentration of the employed dye, the fluorescence intensity data were normalised by calculating the intensity ratio at 626 nm and 656 nm. The evaluation approach for CSCT200 at 50 °C, 65 °C, and 80 °C is illustrated in Fig. 6.

Ratios exceeding 1.0 indicate that the fluorescence spectra exhibit a shift in the intensity maximum from approximately 656 nm to 626 nm wavelength. The intensity ratios over concentration for the various buffer systems and temperatures are presented in Fig. 7.

The shift in Nile Red intensity maximum from 656 nm to 626 nm depends on temperature and P188 concentration. The I_{626}/I_{656} intensity ratio increases in all buffer systems at a specific concentration. As temperature increases, the concentration of P188 required to induce a shift in the fluorescence maximum decreases. At elevated temperatures, a reduced quantity of P188 is necessary to facilitate the formation of a hydrophobic compartment within the solution. Nile Red has an n-octanol–water partition coefficient (logP) value of 3.8, as reported in reference [61], and fast partitioning into micelles is expected [62]. The modified physicochemical environment within the micelle results in a blueshift in emission wavelength and a fluorescent behaviour similar to that observed in ethanol [62]. Furthermore, Fig. 7 illustrates the influence of the solutes in the P188 solutions. A comparison of the buffer systems with 20 mg·mL^{-1} P188 reveals that the presence of solutes reduces the temperature required to induce a shift in the intensity maximum. While no significant shift is observed in pure water (W) at 50 °C, the ratio begins to lift off in CSC at 50 °C. The change at 50 °C is more pronounced for P188 at 20 mg·mL^{-1} in the presence of 200 mM trehalose. With 400 mM trehalose, the increase in intensity ratio reaches approximately 1.0 at 50 °C. The addition of 800 mM trehalose reduces the shift temperature to 37 °C, while at 50 °C, the plateau ratio is reached. It was found that temperatures of 5 °C and 15 °C were insufficient to induce an increase in ratio at any investigated P188 concentrations. Conversely, at 80 °C, a shift in maximum is observable for all buffer systems within the investigated concentration range.

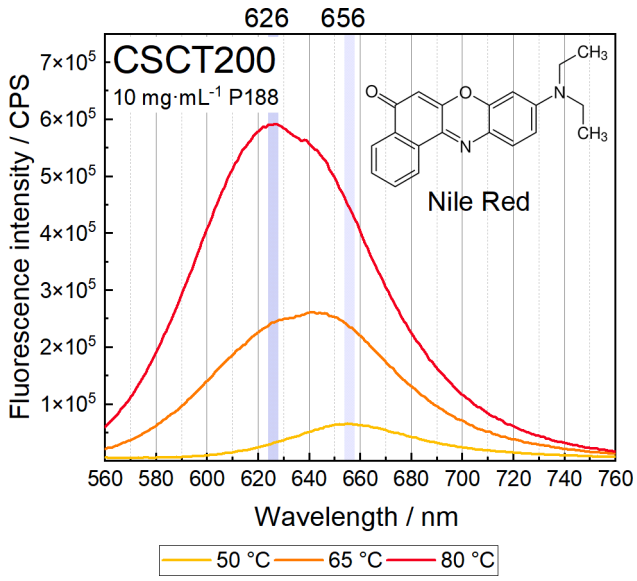

Fig. 6. Nile Red fluorescence spectroscopy results of 10 mg·mL^{-1} P188 in CSCT200. The excitation wavelength was 550 nm, and emission spectra were obtained from 560 nm to 760 nm in 0.5 nm steps. Wavelengths of 626 nm and 656 nm used for ratio calculation are highlighted. The shift in intensity maxima and fluorescence intensities with increasing temperature is visible.

4.3.2. *Comparison with the Pyrene 1:3 ratio method*

Pyrene is commonly employed for CMC determinations, and an evaluation method (1:3 ratio) is described in the literature [63,64]. P188 measurements in CSCT200 were conducted to facilitate a comparative analysis with the findings from Nile Red experiments. The calculated ratio of fluorescence intensities at the first (I_1) and third (I_3) maxima is indicative of the formation of a more hydrophobic micelle core [63,64]. In this instance, the maximum fluorescent intensity observed between 370 nm and 374 nm (I_1) and that observed between 390 nm and 394 nm (I_3) were employed to calculate a ratio. The evaluation approach is exemplified for CSCT200 at 50 °C, 65 °C, and 80 °C in Fig. 8.

Fig. 9 illustrates a comparable trend to that observed in Nile Red measurements. Once more, the data indicates that a temperature of 50 °C and a concentration 20 mg·mL^{-1} are optimal for initiating a discernible shift in the ratio. Moreover, no detectable alteration in the intensity ratio was observed at temperatures between 5 °C and 25 °C. At 65 °C and 80 °C, with a P188 concentration of 20 mg·mL^{-1}, the ratio reached a plateau in both Nile Red and Pyrene experiments.

In the case of Nile Red, a shift in emission maximum to a lower wavelength and an increase in fluorescence intensity can be observed when the dye is dissolved in a nonpolar solvent or a more lipophilic compartment. The evaluation approach is suitable for monitoring alterations in the micro-environment of the dye at different temperatures and in varying buffer compositions. The second dye under investigation, Pyrene, displays a distinct effect when dissolved in a more lipophilic phase. The absolute intensities remain primarily unaltered, yet the ratio of the three discernible emission maxima undergoes a notable change. In contrast to Nile Red, no significant shift in the maximum wavelengths was observed. The behaviour of Pyrene observed in this study is consistent with that previously described in the literature and has been used to determine CMC [20,65]. In this study, the ratio of the first and third maxima was an effective method for visualising the variation in the dye's surroundings.

The alteration of both dyes' fluorescence spectra in response to temperature and concentration changes suggests changes in the micro-environment [66,67]. The shifts in the emission spectra indicate the formation of a more nonpolar micro-compartment, which indicates micelle formation. The immediate increase in the intensity ratio can be attributed to the dye concentration exceeding the critical micelle concentration (CMC) or critical micelle temperature (CMT). The use of Nile Red and Pyrene was found to be an effective method for detecting the effects of increasing temperatures on P188 solutions. The alterations in the fluorescence characteristics of the two dyes are distinct (a shift to lower wavelengths and an increase in intensity, as opposed to a change in the intensity ratio) [66,67]. Nevertheless, identical outcomes were yielded by the two methodologies, thereby substantiating the formation of micelles at a specific P188 concentration and temperature. The similarity of the results for the two probes makes dye-specific artefacts unlikely. Furthermore, this verifies the assumption that a hydrophobic compartment forms at a specific temperature in a P188 solution.

4.3.3. *Examination of the interfacial behaviour by surface tension measurement*

Fig. 10 illustrates the relative surface tension of P188 at a concentration range of 0.0002 mg·mL^{-1} to 160 mg·mL^{-1}, utilising the solvents delineated in Table 1. The surface tension at a specific P188 concentration undergoes a pronounced decline compared to the pure solvent. In particular, between 5 °C and 50 °C, the influence of P188 concentrations below 0.001 mg·mL^{-1} is minimal compared to the pure solvent. At 65 °C and 80 °C, a reduction in relative surface tension is evident at lower P188 concentrations. The relatively sharp decrease in relative surface tension then gives way to a concentration range with smaller decrease rates. At 25 °C and below, the relative surface tension decreases with increasing P188 concentration.

As temperature increases, the curve progression transforms a high P188 concentration. Subsequently, a pronounced decline in relative surface tension is observed, followed by a relatively broad concentration range where the relative surface tension decreases gradually. This ultimately leads to the formation of a plateau. In the case of CSCT400 and CSCT800, this phenomenon can be observed at 37 °C. CSC and CSCT200 demonstrate this behaviour from 50 °C onwards. In the case of water (W), the relative surface tension at high concentrations can be described as constant at temperatures above 65 °C. Notably, P188 displays a pronounced local minimum in pure water from 50 °C onwards. A similar minimum is observed for CSCT400 and CSCT800, although it is less pronounced in CSC and CSCT200.

At the lowest concentrations of approximately 0.0002 mg·mL^{-1}, the P188 concentration on the surface does not result in a quantifiable change in surface tension. This finding is in agreement with the critical micelle concentration (CMC) theory, which posits that most molecules are in equilibrium with the water–air interface. Yet, they do not lower the surface tension due to insufficient surface coverage. An additional increase in surfactant concentration results in a pronounced decline in the logarithmic plotted surface tension curves. The equilibrium between the solute molecules within the solution and at the surface significantly influences this point, in addition to the absolute surfactant concentration. Consequently, the distribution is contingent upon the hydrophilic and lipophilic characteristics inherent to the surfactant molecule. With an HLB value of 29 (on the Davies scale), P188 is characterised as a highly hydrophilic surfactant. This leads to the hypothesis that at low concentrations, a relatively large amount of P188 is detectable in the subphase rather than at the interface. As temperature rises, the interaction between the PEO segment of P188 and the surrounding water decreases. This phenomenon can be attributed to the heightened temperature sensitivity of hydrogen bonds between water and the surfactant compared to nonpolar interactions. This assertion is supported by the findings of several studies, including those referenced in citations [19,31,68]. Consequently, the theoretical HLB value decreases with increasing temperature, whereby the lipophilic fraction exerts a greater influence. At elevated temperatures, low P188 concentrations reduce surface tension due to a shift in the equilibrium between the subphase and the interface towards the latter. This explains the observed trend of decreasing surface tension at lower concentrations with increasing temperature, as illustrated in Fig. 10.

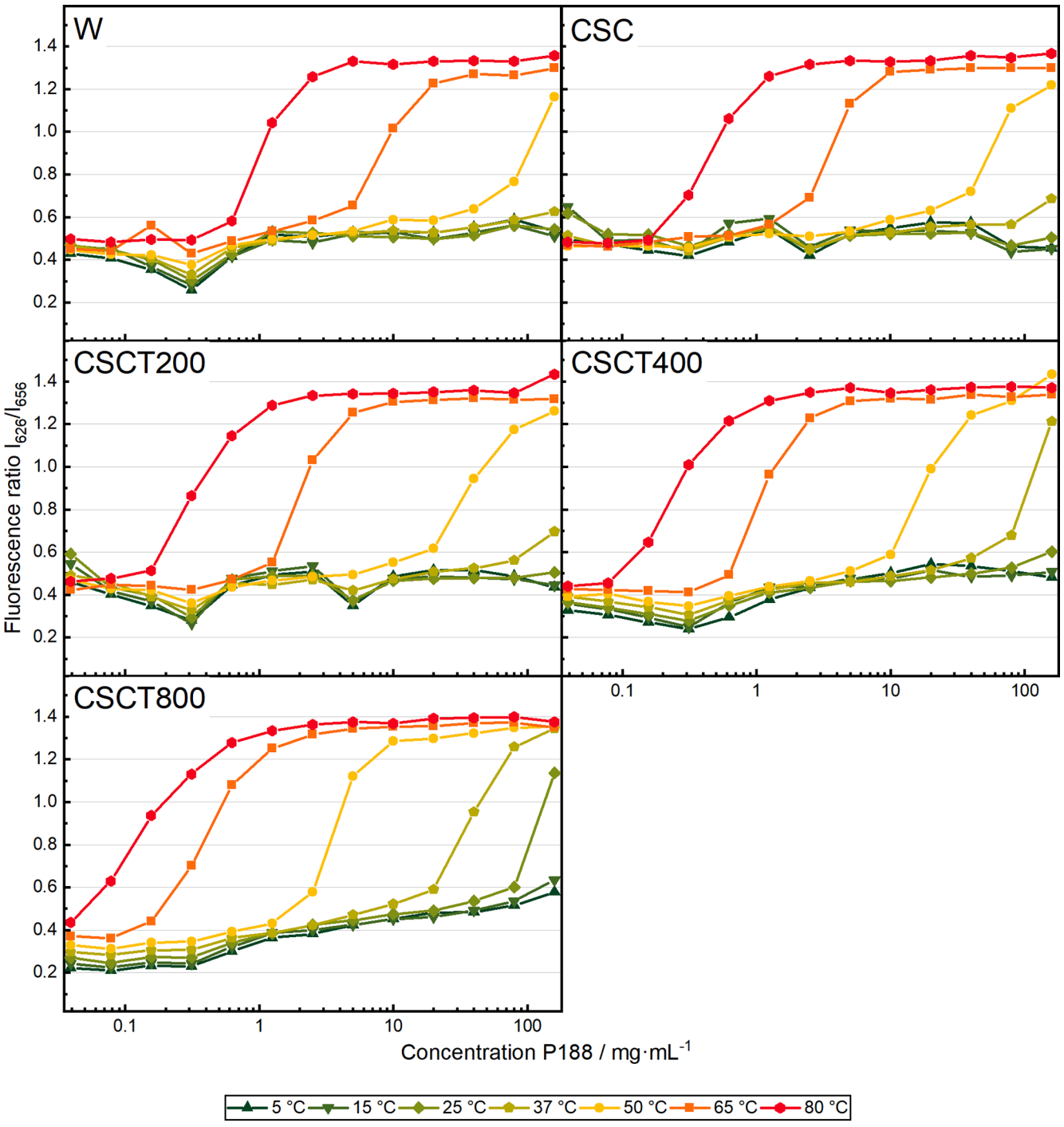

Fig. 7. Results of Nile Red fluorescence experiments. P188 concentrations from 0.039 mg·mL^{-1} to 160 mg·mL^{-1} are shown in water (W), citrate buffer plus sodium chloride (CSC), citrate buffer plus sodium chloride containing 200 mM (CSCT200), 400 mM (CSCT400), and 800 mM trehalose (CSCT800). The ratio was calculated from the intensities of 626 nm and 656 nm.

With increasing surfactant concentration, the water–air interface is covered by additional surfactant molecules. Following the CMC description, the progressive saturation of the interface reaches a specific concentration at which surfactant molecules cover the entire surface. At this point, the minimum surface tension can be measured. Further addition of surfactant leads to the formation of micelles, as the interaction of surfactant molecules in the solution is now favoured [45]. Above the surfactant concentration defined as CMC, the surface tension remains constant.

For the investigated P188 samples, the described ideal curve was not found for temperatures between 5 °C and 25 °C. In contrast to the anticipated outcome, the relative surface tension does not reach a constant value; instead, it continues to decrease with an increase in P188 concentration. This indicates that the surface is not in saturation following the inflection point (decrease in negative slope). It has been documented in the literature that poloxamers, which are polymeric surfactants, can form a variety of conformations when they interact at interfaces. As surface pressure increases, poloxamer molecules at the air-water interface undergo compression, forming various conformations, including pancake, mushroom, and brush conformations [69–71]. At low concentrations, P188 molecules exhibit the capacity to disperse over a considerable surface range, accompanied by an increase in the number

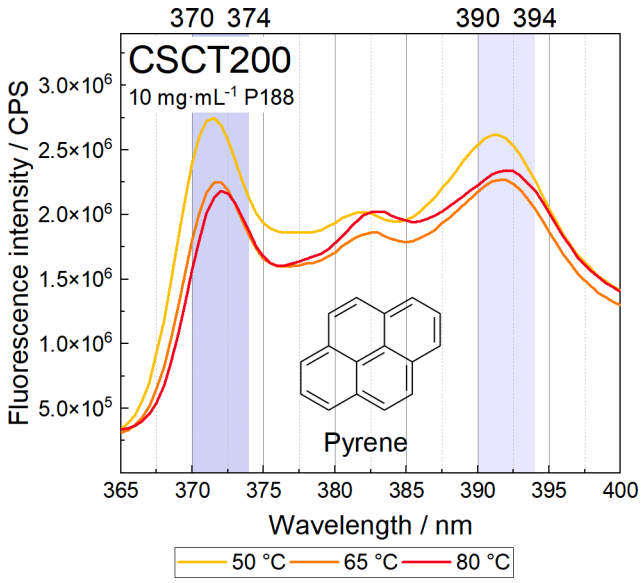

Fig. 8. Results of Pyrene fluorescence spectroscopy of 10 mg·mL^{-1} P188 in CSCT200. The excitation wavelength was 336 nm, and emission spectra were obtained from 350 to 500 nm in 1 nm steps. Maximum intensity was identified in the highlighted ranges of 370–374 nm (I_1) and 390–394 nm (I_3) wavelength and used for ratio calculation.

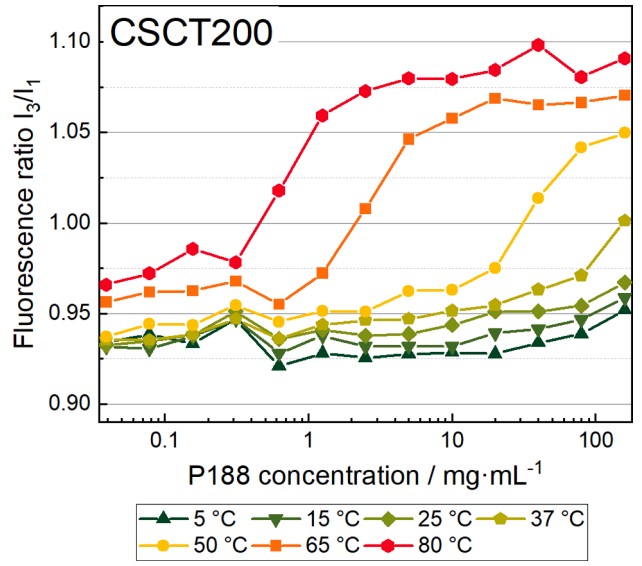

Fig. 9. Results of Pyrene fluorescence experiments. P188 concentrations from 0.039 mg·mL^{-1} to 160 mg·mL^{-1} are shown in citrate buffer plus sodium chloride containing 200 mM (CSCT200). The ratio of Pyrene intensities bands 3 (I_3) and 1 (I_1) were used for ratio calculation.

of folds as the area per molecule diminishes. Consequently, at lower temperatures, the preferred behaviour of P188 is a change in its air-water conformation from pancakes into mushrooms, accompanied by a decrease in the area per molecule. This is to avoid an excess of P188 molecules [70,71]. As the level of surface saturation increases further, it becomes impossible to identify a constant level of relative surface tension resulting from micelle formation.

At elevated temperatures, the recorded curves approximate the idealised CMC curve, demonstrating a localised state of supersaturation and, subsequently, a constant relative surface tension. Attaining this equilibrium of surface tension signifies that the surface has reached saturation and the area per molecule has been reduced to a minimum. The brush conformation at the interface is attained, indicating that the surface is fully saturated. It follows that the dimensions of the P188 molecule at the interface cannot undergo a further reduction. At that point, an additional 188 is either dissolved in a monomolecular state within the solution or commences the formation of micelles. A plot of the surface tension versus concentration in a logarithmic manner may indicate the CMC value by identifying a local minimum or employing the tangent method. The data in question are not suitable for making a statement regarding micelle formation, as the interactions at the interface are monitored, but not the interactions between the surfactant molecules within the solution. The data demonstrate that no idealised surface tension curve can be observed for P188 at temperatures below 37 °C. Given that no constant level of relative surface tension is reached, it seems probable that further saturation of the interfaces by conformational changes will occur. The concentration of P188 in the subphase exhibits a parallel increase without the formation of micelles.

4.3.4. Polarity and micro-viscosity by electron paramagnetic resonance spectroscopy (EPR)

Electron paramagnetic resonance (EPR) spectroscopy was employed to investigate the concentration-dependent behaviour of P188 (0.039–160 mg·mL^{-1}) in CSCT200 buffer, using the hydrophobic spin probe Tempolbenzoate. Fig. 11 shows the recorded EPR spectra in pure CSCT200 buffer and in the presence of 10 mg·mL^{-1} P188 at temperatures of 50 °C, 65 °C, and 80 °C. No notable changes were discerned in the pure buffer upon temperature elevation. This suggests that the micro-environment remained unaltered with temperature fluctuations. However, when 10 mg·mL^{-1} P188 were added to the solution, notable differences in the spectra were observed. At 50 °C, the P188 spectra exhibit no discernible differences from those of pure water. However, at 65 °C, the maximum signal amplitudes, particularly of the third peak, show a notable decline. The signal amplitude decrease, especially of the third, can be caused by two contributions: (i) an increase of the local viscosity and (ii) the distribution of the spin probe in several microenvironments with different polarities. An increase in viscosity would only lead to broader lines but not to an asymmetric line shape. The spectral analysis shows that both factors (viscosity and distribution to different microenvironments) contribute to the observed changes in the spectral shape. An increase in the spin probe's rotational correlation times (τ_c) is evident, resulting in a broadening of the peaks. Fig. 11 demonstrates that the signal amplitude decreases, and broadening becomes more pronounced at 80 °C. The asymmetry of the third signal within the spectra of 10 mg·mL^{-1} P188 at 65 °C and 80 °C is evident. This phenomenon is caused by the superimposition of two spectral components of the spin probe Tempolbenzoate, indicating the localisation of the latter in a hydrophilic and a hydrophobic microenvironment. Fig. 12A shows the spectra of 10 mg·mL^{-1} P188 at 80 °C and the corresponding two-component-fit. The total fit (red line above the raw data) is composed of the spectra of the hydrophilic and hydrophobic species (Fig. 12A, bottom: blue and orange line) in a 1:1 proportion. The hydrophilic component's more extensive hyperfine splitting (distance between the peaks) is clearly discernible. Fig. 12B illustrates the ratios of the maximum and the minimum values within the third peak for P188 concentrations spanning a range of 160 mg·mL^{-1} to 5 mg·mL^{-1} at temperatures between 5 °C to 80 °C. At a specific temperature, the third peak exhibits a maximum/minimum ratio that is discernibly below 1.0, indicating the presence of asymmetry in the signal. The ratio is approximately 1.0 at a higher temperature, as the hydrophobic species now predominates. To illustrate, the third peak of a 40 mg·mL^{-1} P188 solution becomes asymmetrical at a temperature of 50 °C, indicating the existence of a hydrophobic species alongside the hydrophilic one. At 65 °C, the third peak reverts to a symmetric profile, reflecting the dominance of the hydrophobic species.

Following the demonstration of the transition from a hydrophilic to a hydrophobic species at a specific temperature, the rotational correlation time (τ_c) and nitrogen isotropic hyperfine coupling constant (A_N) are

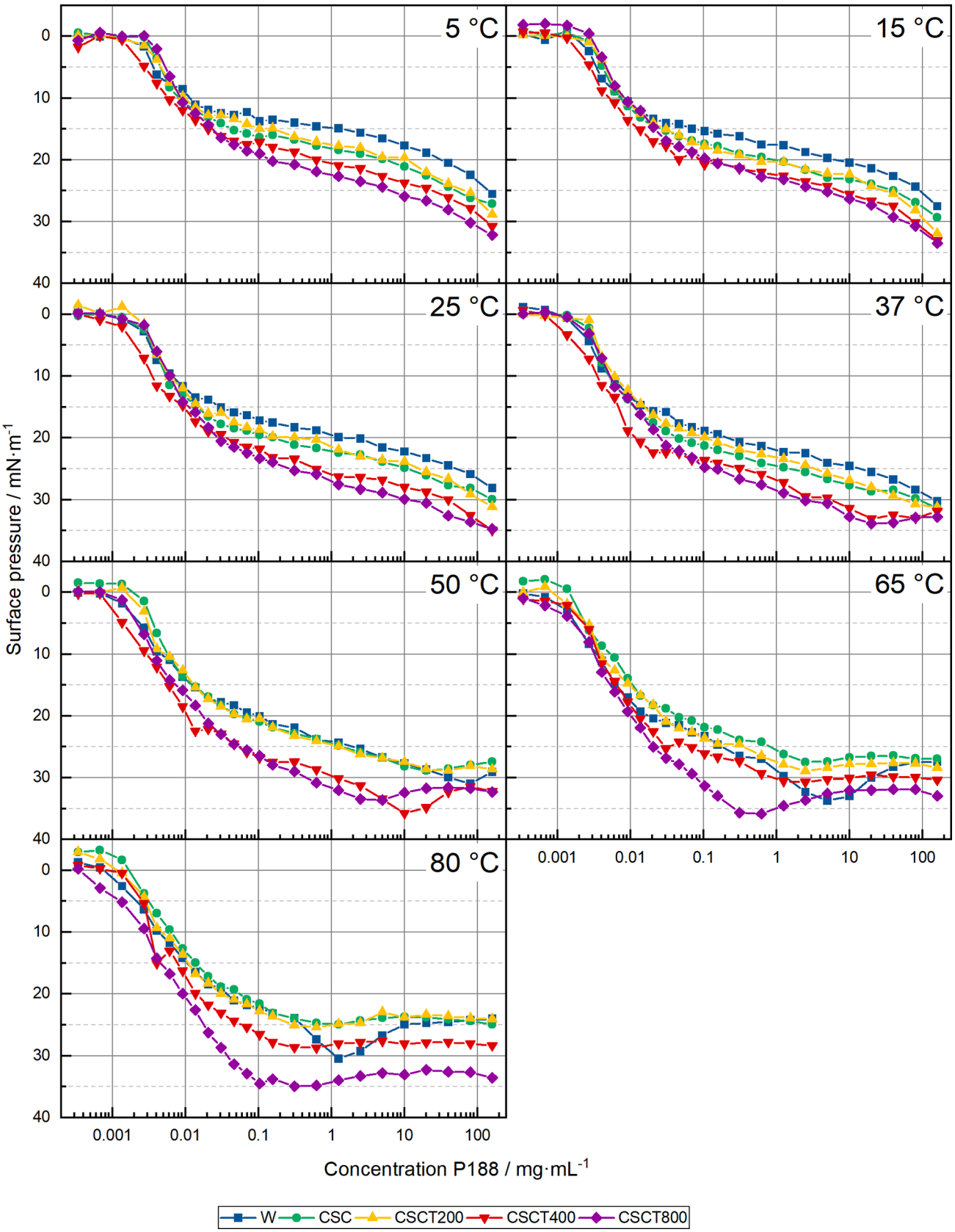

Fig. 10. Results from drop shape analysis: Relative surface tension is calculated by subtracting the pure buffer surface tension from the sample surface tension. Relative surface tensions of P188 concentrations from 0.00034 mg·mL^{-1} to 160 mg·mL^{-1} are depicted at 5 °C, 15 °C, 25 °C, 37 °C, 50 °C, 65 °C and 80 °C. P188 in water (W), citrate buffer plus sodium chloride (CSC), citrate buffer plus sodium chloride containing 200 mM (CSCT200), 400 mM (CSCT400), and 800 mM trehalose (CSCT800).

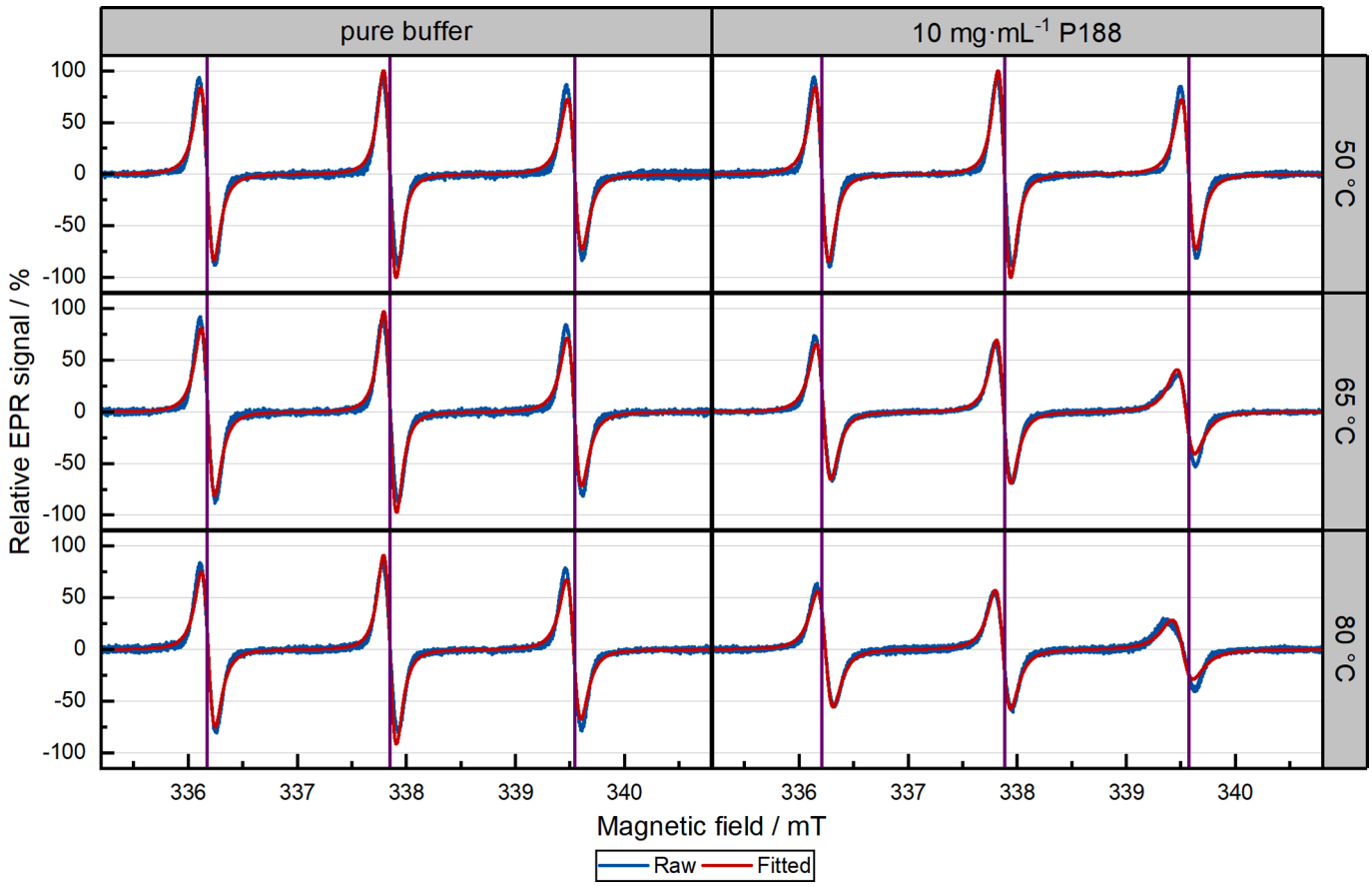

Fig. 11. Electron paramagnetic resonance (EPR) spectra of Tempolbenzoate in pure buffer (25 mM citrate, pH 6; 115 mM sodium chloride; 200 mM trehalose) in contrast to 10 mg·mL^{-1} P188 in 25 mM citrate, pH 6; 115 mM sodium chloride; 200 mM trehalose. Temperatures were set to 50 °C, 65 °C and 80 °C. Raw data are shown in blue, and fitted data is in red.

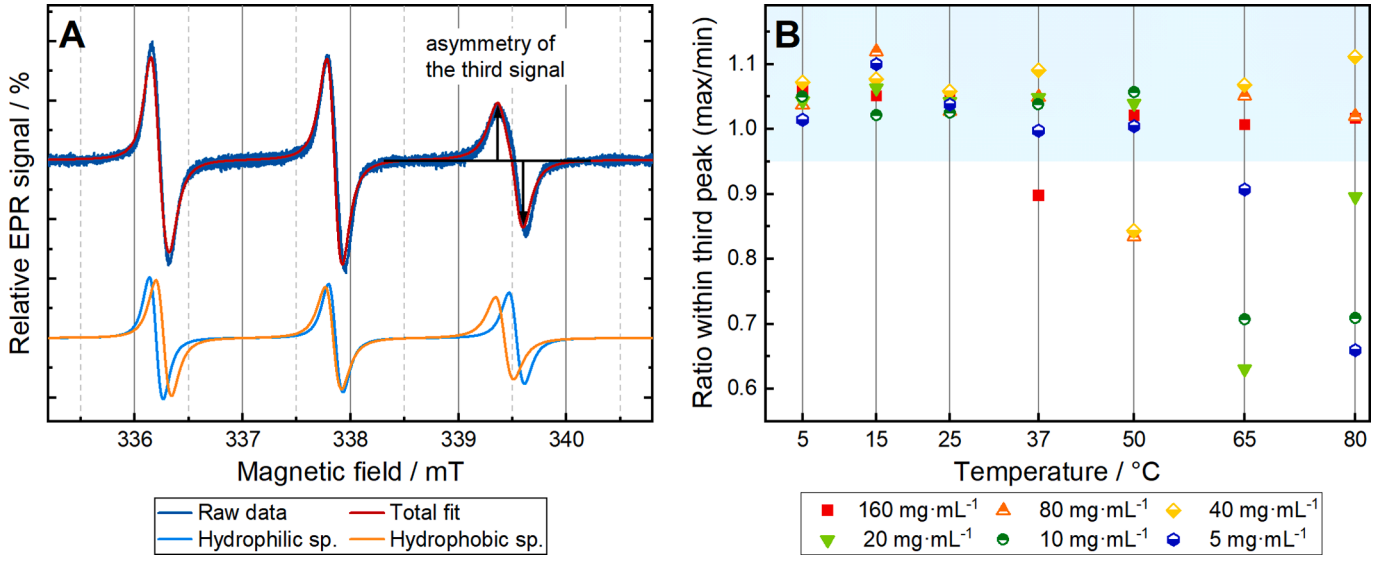

Fig. 12. A) Two-component fit of electron paramagnetic resonance (EPR) spectra due to asymmetry of the third signal. Two species of Tempolbenzoate are distinguished within the total fit (red line in the upper spectra). The total fit is composed of a hydrophobic (orange line) and a hydrophilic (blue line) species (in the lower spectra). **B)** Max/Min Intensity ratios within the third EPR peak. Values below 0.95 indicate asymmetrical third signals and the superimposition of the signals of two components.

calculated using the one-component fits. This may indicate that the calculations conducted at the transition temperature are not precise. However, a change in the selected parameters can still be determined, allowing for the identification of differences in the chemical environment of the spin probe. Fig. 13 illustrates the discrepancies in τ_c and A_N between the pure CSCT200 buffer and the P188-containing samples. A

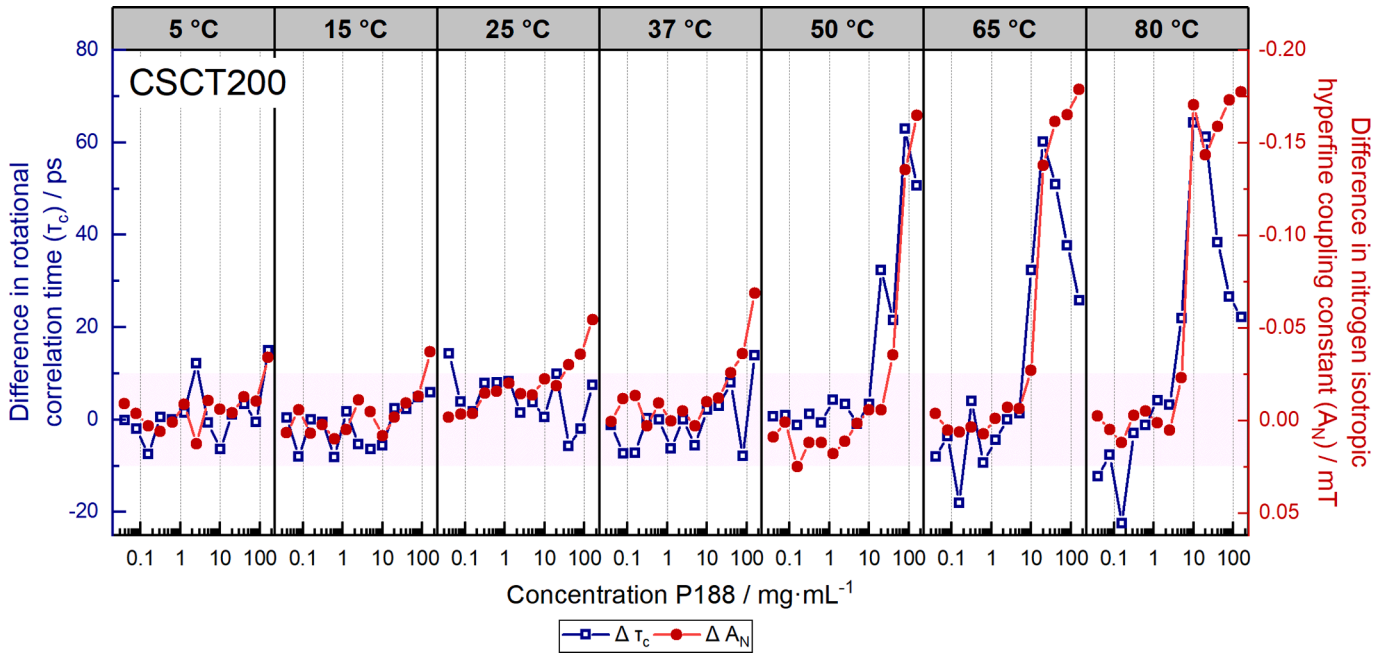

Fig. 13. Results from electron paramagnetic resonance (EPR) spectroscopy: The distance of the outer signals (A_N) and rotational correlation time (τ_c) was calculated from the fitted data. The difference in A_N (red, filled circles) and τ_c (blue, unfilled squares) of samples containing 0.039 mg·mL^{-1} to 160 mg·mL^{-1} P188 to the P188-free CSCT200 buffer is depicted. P188 samples were investigated at 5 °C, 15 °C, 25 °C, 37 °C, 50 °C, 65 °C and 80 °C.

shift in both τ_c and A_N was observed at temperatures between 50 °C and 80 °C. At 50 °C, the shift occurs at concentrations ranging from 20 mg·mL^{-1} to 40 mg·mL^{-1}. At 65 °C, the shift occurs at a concentration of 10 mg·mL^{-1}, while at 80 °C, the shift occurs at a concentration of 5 mg·mL^{-1}.

Similar to alterations in the fluorescence emission spectra, EPR spectra of nitroxide spin probes are sensitive to changes in their microenvironment. As the signals of the excited electrons are susceptible to alterations in micro-viscosity, the uptake of the probe in micelle cores results in discernible shifts in the spectra [39,40]. As alteration in τ_c indicates a change in the viscosity of the compartment where the probe is present, the results demonstrate the formation of a micro-compartment with a higher micro-viscosity.

In addition, the nitrogen isotropic hyperfine coupling constant indicates the polarity of the nitroxide environment. A reduction in the A_N value is indicative of an increase in hydrophobicity. The polar solvent water facilitates the polarisation of the N–O bond in Tempolbenzoate. This increases electron spin density at the nitrogen, which in turn leads to an increase in A_N [38,39].

Conversely, the distribution of Tempolbenzoate in nonpolar micelle cores leads to a comparable decrease in A_N, as observed in a nonpolar solvent (e.g., lipophilic triglycerides) [72]. These results suggest the formation of a more hydrophobic and water-free compartment within the solution. As the shifts in both indicators occur in parallel, the formation of a hydrophobic compartment is associated with an increase in viscosity compared to that of pure buffer. This is consistent with the concept of micelle formation, whereby an increase in hydrophobicity and viscosity is anticipated [73,74]. The use of both τ_c and A_N as indicators for the critical micelle concentration is described in the literature [39,40,75,76]. In the case of P188, following the pronounced decline in A_N and the surge in τ_c, A_N values exhibit minimal fluctuation while τ_c values begin to decline once more. Consequently, the micro-viscosity decreases while the polarity of the probe's environment remains constant. It can be postulated that the formation of micelles results in a more viscous structure that becomes more flexible when the concentration of P188 is increased. An alternative explanation for these observations is that alterations in micelle shape are responsible. An increase in spherical shape at elevated concentrations facilitates enhanced micelle rotation. The polarity within the micelle core remains predominantly hydrophobic, while the mobility of Tempolbenzoate solubilised in P188 micelles increases with rising P188 concentrations. The slight increase in particle size at these concentrations suggests a minor growth in micelle size. It is reasonable to posit that an increase in micelle and core size may contribute to the enhanced mobility of the probe.

4.3.5. Nuclear Magnetic Resonance Spectroscopy (NMR)

The results of the ^{1}H-NMR spectra of 40 mg·mL^{-1} P188 in D_2O are depicted in Fig. 14. The assignments of the signals were studied in detail by Ma et al. (2006) [37] and were subsequently adopted to evaluate the spectra. A distinct change in the chemical shift of the EO-CH_2- signal was discerned at temperatures exceeding 65 °C. Additionally, the width of the signal increases at elevated temperatures. The PO-CH_2- signal exhibits a pronounced hyperfine structure at temperatures below 65 °C, which subsequently merges and disappears at higher temperatures. Furthermore, a change in chemical shift is observed, accompanied by the emergence of an additional signal within the range of 3.45 ppm to 3.30 ppm. The triplet observed at approximately 3.63 ppm can be attributed to free PEO impurities [37]. The PO-CH_3 signal exhibits a triplet at low temperatures, which broadens and shows a higher field shift at higher temperatures. Fig. 15 illustrates the chemical shifts, as well as the line width (half-height width) for the EO-CH_2- and PO-CH_3 signals (with the highest intensity within the depicted range) and the integral value of the additional peak in the PO-CH_2- region.

The results obtained in this study are similar to those reported by Ma et al. (2006 and 2007) [37,77] in that an abrupt change in the chemical shift of the PO-CH_3 protons was observed, concomitant with a broadening of the initial triplet, which was visible at the half-height width of the peak. As previously discussed, the upfield shift can be attributed to the varying magnetic susceptibility of protons transferred into a non-polar environment [37,78]. The increase in the half-height width of the PO-CH_3 protons suggests a reduction in the mobility of the PPO blockchain at elevated temperatures. Given the rapidity and lack of graduality of the observed decrease in mobility, the spontaneous association of the polymer chains into micelles is postulated. The alteration in polarity and the reduction in mobility of the PO-CH_3 protons indicate the CMT of P188 in D_2O. Additionally, the integral of the PO-CH_2- signal

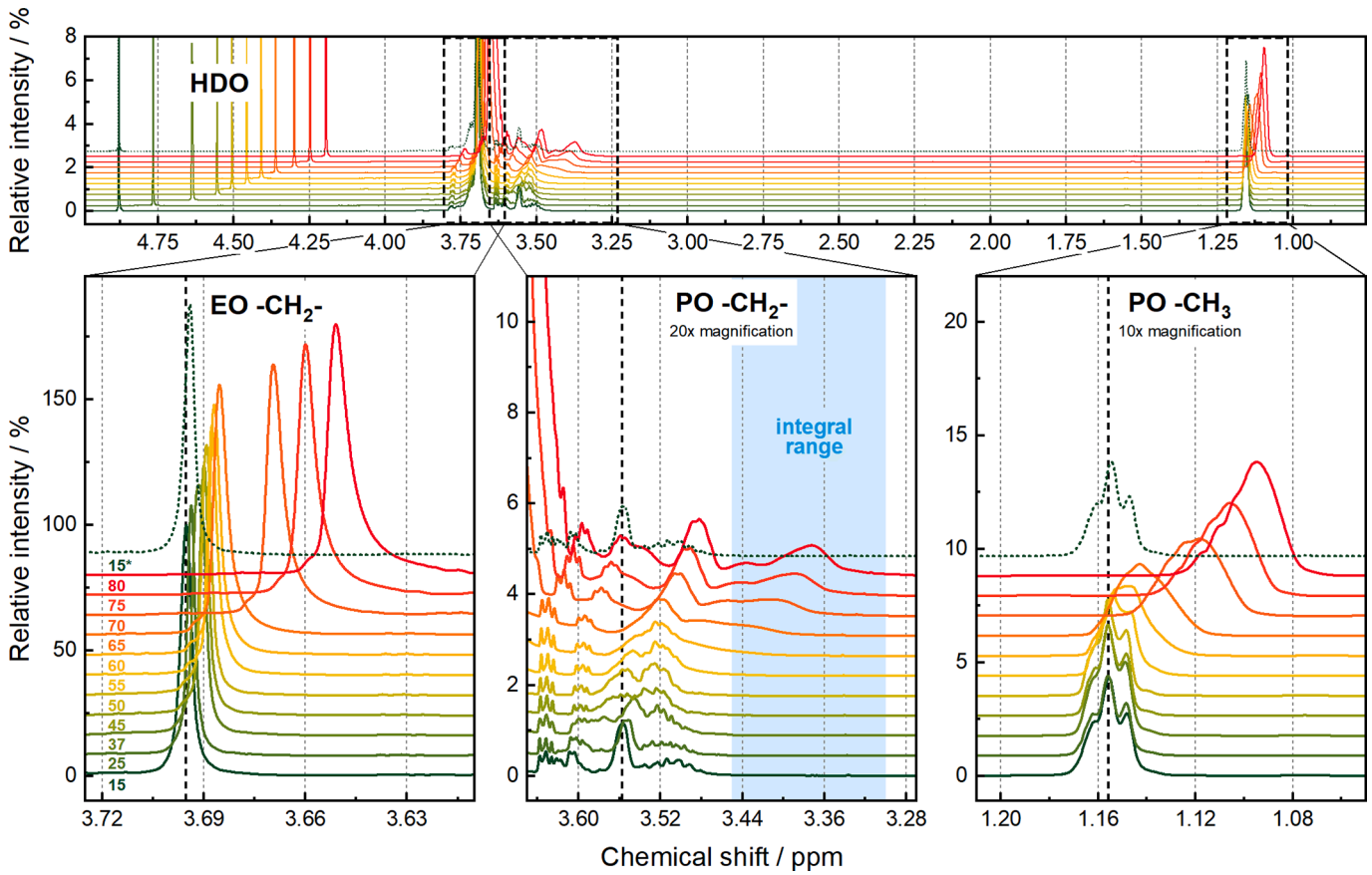

Fig. 14. ^{1}H-nuclear magnetic resonance (^{1}H-NMR) spectra of 40 mg·mL^{-1} P188 in D_2O at temperatures ranging from 15 °C to 80 °C. Regions relevant to the evaluation are zoomed in. The integral range for the signal in the PO-CH_2- region is highlighted in light blue. The dotted dark green line shows the control spectra at 15 °C after cooling down from 80 °C. Characteristic peaks are marked with a dotted line to guide the eye.

is displayed in Fig. 15. The separation of the complex signal in the range of 3.65–3.30 ppm, in conjunction with the loss of hyperfine splitting, has been described for poloxamers at elevated temperatures [51,77]. The observed increase in the integral value is attributed to the disruption of intramolecular hydrogen bonds between PO-CH_2- and the ether oxygen.

The disruption of the intramolecular interactions leads to a conformational change from gauche to the trans conformation of the stereocentre in PPO [77]. This change in conformation and the dehydration processes were also described in studies using Raman [79] or infrared spectroscopy [80]. As a consequence of the trans conformation providing a distinct chemical environment for the PO-CH_2- protons, the integral of the trans signal is observed to increase. In summary, the PPO core of the formed micelles is almost entirely dehydrated, with strong interactions between the PPO chains and restricted mobility of the PO-CH_3 [79,80]. This is consistent with our findings, which revealed restricted mobility, a more nonpolar environment of the PO-CH_3, and a change from gauche to trans conformation of the PO-CH_2- element. Notably, the mobility-indicating half-height width appears to increase prior to the polarity-indicating chemical upshift. This could suggest a more restricted mobility of the PPO chain before dehydration and a nonpolar micelle core formation.

In contrast to the PPO block, the PEO block retains a degree of hydration even when the interaction with water is reduced. Ma et al. (2007) observed an upfield shift of the EO-CH_2-NMR (^{1}H) signal as temperature increased, concluding that the environment of the PEO block remains largely unaltered and in contact with the surrounding water during micelle formation [77].

In the present study, a slight upfield shift was also observed between 15 °C and 65 °C. However, at temperatures exceeding 65 °C, a pronounced decline in the chemical shift was observed. In light of the aforementioned discussion of the PPO signals, this suggests the occurrence of dehydration processes and the formation of a more nonpolar environment within the PEO blocks. Furthermore, an alteration in the mobility of the chains was discerned, as evidenced by an increase in the half-height width of the EO-CH_2- signal.

The reduction in mobility is not as pronounced as observed for the PPO block. However, an increase in the half-height width of the EO-CH_2- signal was observed to correlate with the liquid crystallisation temperature, defined as the temperature at which poloxamers form a liquid-crystalline cubic phase [77]. This phase can be described as a close packing of micelles, accompanied by an interaction between the PEO chains.

For Pluronic F88, which is as hydrophilic as P188 but with a higher average molecular weight (11′400 versus 8′400 Da) [58], the liquid crystallisation temperature was above 60 °C for a 200 mg·mL^{-1} solution [77]. In this study, a markedly lower P188 concentration of 40 mg·mL^{-1} was used, which renders the likelihood of a decrease in mobility and dehydration of the corona greater than that of the formation of a liquid crystalline phase.

It can be concluded that, in the case of P188, there is a certain degree of dehydration of the PEO block, and the chains are slightly more rigid when associated with a micelle. This is consistent with the Raman and infrared spectroscopy findings for other poloxamers [79,80]. As previously observed for the PPO block, mobility changes become evident before the onset of dehydration. The association of P188 molecules in a 40 mg·mL^{-1} solution may occur at temperatures above 60 °C. However, the drying of the micelle core and the partial drying of the PEO corona may begin at temperatures above 70 °C. The results of the T_{max} and T_{Onset} determinations are highlighted in Fig. 15, which depicts the range between these two temperature values. In both cases, for both EO-CH_2-

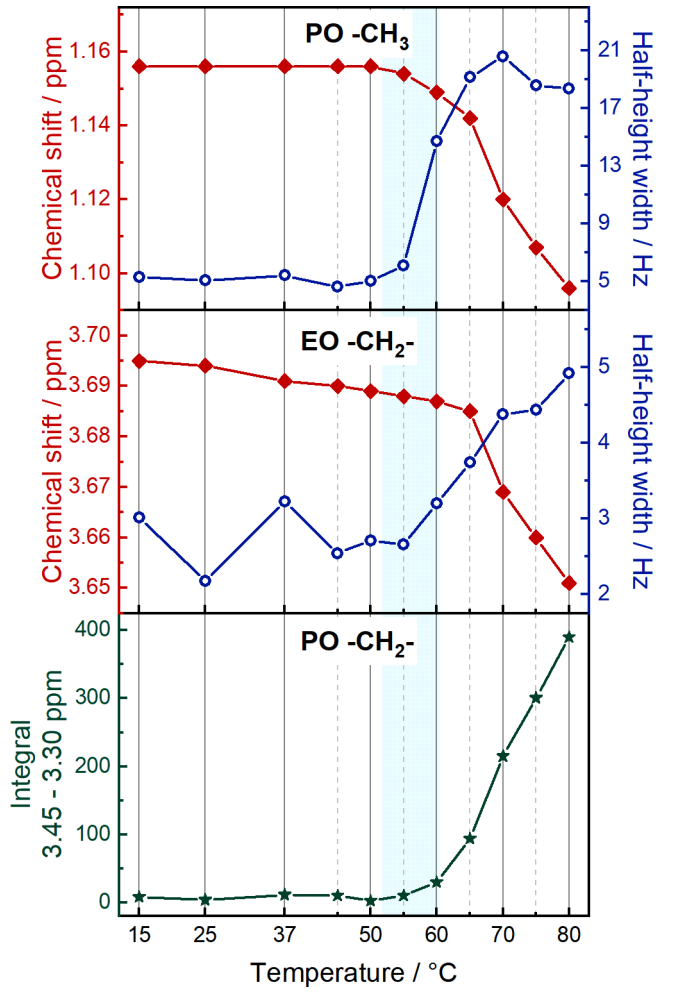

Fig. 15. Chemical shift and half-height of the PO-CH_3 and EO-CH_2- signals in the ^{1}H-NMR spectra, as well as the absolute integral value between 3.45 ppm and 3.30 ppm of the PO-CH_2- region. The integral region is highlighted in Fig. 14. Corresponding T_{max} and T_{Onset} of 40 mg·mL^{-1} are highlighted in light blue.

and PO-CH_3, a decrease in mobility, expressed as an increase in half-height width, is observed within this temperature range. Interestingly, the reduction in the PO-CH_3 signal is almost complete within this range, while the mobility continues to decrease with increasing temperature. It should be noted that CMT values in H_2O are reported to be slightly lower by 2–3 °C [77]. However, the change in chemical shift, indicative of the formation of a 'dry' nonpolar environment and the occurrence of the additional signal between 3.45 ppm and 3.30 ppm, indicative of the percentage of trans conformation of the PPO block, occurs at temperatures above the T_{max}. The unfolding process observed by DSC measurements is thus associated with the formation of molecular assemblies and a decrease in molecular mobility. An additional temperature increase then results in the dehydration of the micelle core, which is subsequently followed by the dehydration of the PEO corona.

Interestingly, all changes in the NMR spectra were fully reversible when the sample was cooled to 15 °C after heating it to 80 °C. This indicates, that the micellisation process was invertible and the analysis was non-destructive.

The results of the ^{13}C-NMR spectra of 40 mg·mL^{-1} P188 in D_2O are shown in Fig. 16. As for the ^{1}H-NMR spectra, the signal assignment was used, as reported by Ma et al. (2006) [37]. Comparable changes in the chemical shifts of the PO-CH_2- and PO-CH_3 signals were observed at elevated temperatures. PO-CH_2- and PO-CH_3 show downfield shifts and a significant broadening at temperatures above 60 °C. In contrast, the complex PO-CH- signal shows a weakening of the hyperfine splitting and a consistent upfield shift with increasing temperature. The signal of the EO-CH_2- carbons shows an upfield shift from 15 °C to 45 °C, followed by an almost constant ppm value. At 70 °C, there is an abrupt decrease in chemical shift and an increase in line width (half-height width). Changes in chemical shift and half-height width for the PO-CH_3, EO–CH_2- and PO-CH_2- signals are depicted in Fig. 17.

Similar to ^{1}H-NMR signals, the half-height width of the ^{13}C-NMR lines can be used as a surrogate for the mobility of the corresponding polymer block chain. Different factors cause changes in the chemical shifts. In analogy to the PO-CH_2- signal in ^{1}H-NMR spectra, the change from gauche to trans conformation impacts the chemical shift. In addition, the polarity of the chemical environment has an indirect effect on the ppm value. The gauche/trans ratio and a non-polar environment lead to downfield shifts and increasing ppm values [37]. For both PO-CH_3 and PO-CH_2- signals, a substantial increase in the ppm value can be observed at 65 °C. At this point, a predominance of the trans conformation and a non-polar environment can be assumed. Thus, the formation of a micelle core by the PPO chains is likely. Interestingly, changes in the half-height width can be observed from 55 °C on. At these temperatures, the PPO structures may become more rigid before further dehydration and the formation of a non-polar core. The decreasing viscosity and the higher mobility within the micelle core at higher temperatures explain the decrease in the line width after reaching a maximum level. For the EO-CH_2- signal, Ma et al. (2006) [37] described possible effects on the chemical shift. For the PO-CH_2- signals, the gauche/trans conformation leads to a downfield shift when the trans conformation predominates. Conversely, changes in hydrogen bonding with increasing temperature would lead to upfield shifts and thus decreased ppm values. For the poloxamers investigated in their study, downfield shifts were observed for the EO-CH_2- signals when comparing monomer and micellar solutions. The researchers concluded that the conformational changes influence the chemical shift more than the hydrogen bonds between water and the PEO. As shown in Fig. 17, the evaluation of the chemical shift of the EO-CH_2- signals shows a different behaviour. The ppm value decreases between 15 °C and 45 °C, followed by constant values up to 65 °C, while the chemical shift continues to decrease from 70 °C to 80 °C. In contrast to the behaviour described above, the influence of the hydrogen bond between water and PEO was found to have a greater effect on the chemical shift. Interestingly, this suggests that the hydrophilic interaction appears to decrease at 15 °C, 25 °C and 37 °C and then remains constant between 45 °C and 65 °C. Only at 70 °C do the hydrogen bonds become weaker again. However, similar to the PPO signals, the half-height width increases at a specific temperature, suggesting a reduced mobility of the PEO chains at 65 °C. Thus, PEO exhibits dehydration and increased stiffness at elevated temperatures. Both effects occur at higher temperatures than required to induce similar effects on the PPO chain. As with the ^{1}H-NMR data, the range between T_{Onset} and T_{max} for 40 mg·mL^{-1} P188 in water is highlighted in Fig. 17. Similar to the proton NMR, changes in the mobility of PO-CH_3 and PO-CH_2- occur mainly within the range shown, while the chemical shift increases at temperatures above T_{max}. However, the half-height width for the EO-CH_2- signal increases at temperatures above T_{max}. In agreement with the ^{1}H-NMR results, changes in the chemical shift of the EO-CH_2- signal occur at 70 °C to 80 °C.

Overall, the NMR data provided information on the chemical environment, mobility, and conformation of both polymer blocks in poloxamer 188 at different temperatures. We were able to detect relatively sharp changes in the NMR signals at temperatures where micelles are expected to form. We conclude that the PPO blocks begin to associate, leading to a decreased mobility of the corresponding cores. At this point, the formed core still contains water. Further temperature increases lead to the dehydration of the PPO cores and the development of a non-polar environment in which the *trans*-conformation of the polymer is favoured. The PEO corona of the micelle shows relatively small changes in mobility and polarity compared to the PPO block. At high temperatures

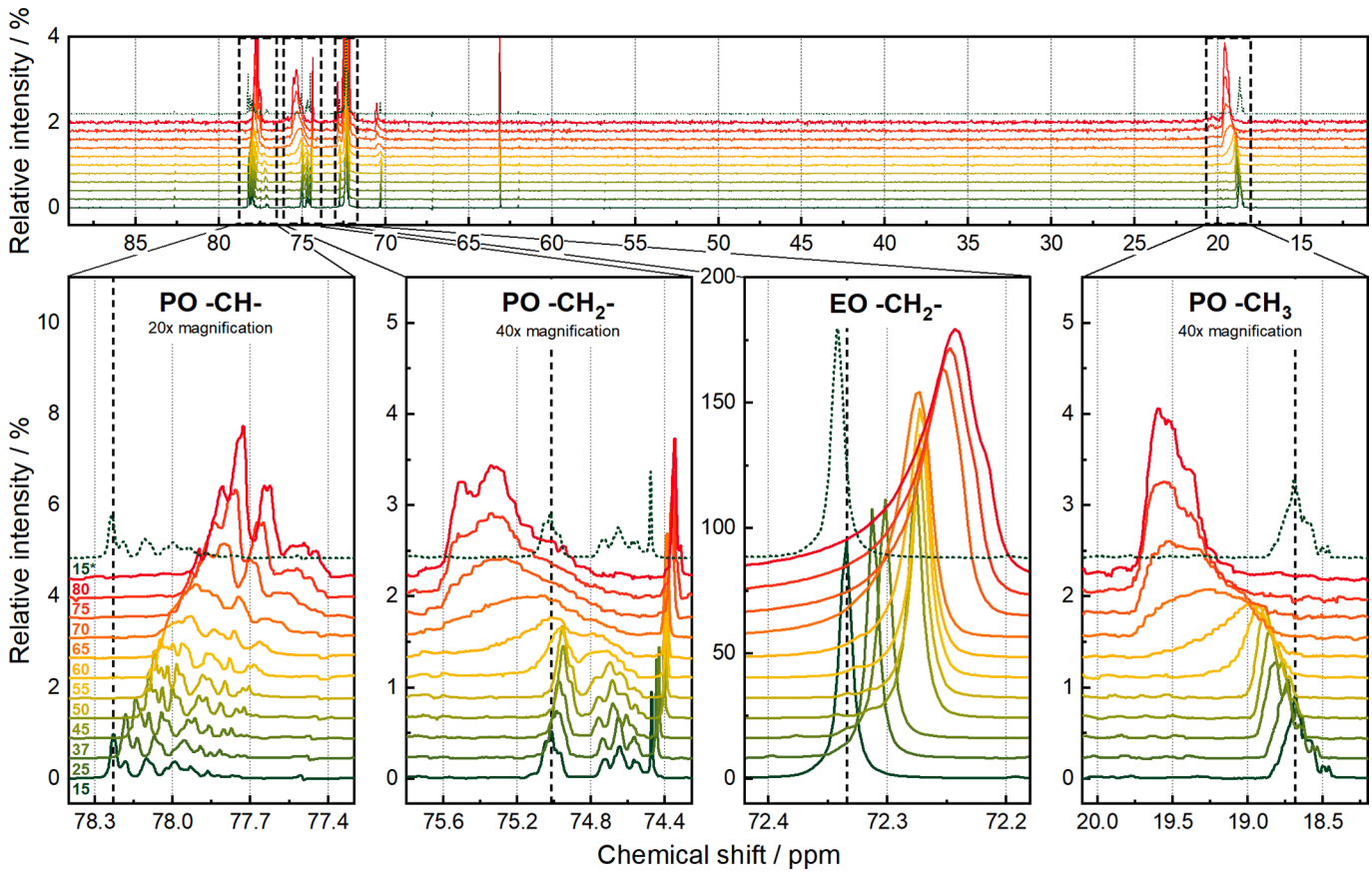

Fig. 16. ^{13}C-nuclear magnetic resonance (^{13}C-NMR) spectra of 40 mg·mL^{-1} P188 in D_2O at temperatures ranging from 15 °C to 80 °C. Regions relevant for evaluation are shown magnified. The dotted green line shows the spectra at 15 °C after an increase of the temperature to 80 °C. Characteristic peaks are marked with a dotted line to guide the eye.

of 70 °C to 80 °C, NMR signals associated with PEO indicate that the chains in the corona show dehydration processes and are also associated with reduced mobility.

4.4. Summarising overview

Fig. 18 shows the overlay of plots for hydrodynamic particle diameter, relative surface tension, Nile Red, Pyrene, and EPR (A_N and τ_c) data. The calculated concentration ranges between T_{Onset} and T_{max} for 37 °C, 50 °C, 65 °C and 80 °C are highlighted (see Table 3). The relationship between the different experimental data and their suitability for detecting changes in the surfactant system in the same concentration range is evident. The concentration range between T_{Onset} and T_{max} fits with the changes observed by the dye methods. The highlighted region covers almost the entire shift in intensity ratios for fluorescence. Additionally, a clear increase in particle size was observed over the described range. The largest slope in the particle size distribution also coincides almost exactly with the area of the local minimum of the surface tension values. This, together with the fact that the minimum is reached between T_{Onset} and T_{max}, indicates that the first micellar structures are formed from this point onwards. As described, the local minimum can be caused by small amounts of hydrophobic impurities from the poloxamer, for example, di-blocks of PEO and PPO. The EPR experiments, which provide information on micro-viscosity changes when the spin probe is partitioned into a hydrophobic compartment, show a decrease in A_N and an increase in τ_c in the highlighted concentration ranges. This can be explained by the described formation of micelles and a hydrophobic compartment into which the lipophilic probe is partitioned. The local viscosity inside the micelle cores is higher than in water, leading to higher τ_c values. Most of the increase in particle size also occurs within the highlighted concentration ranges, supporting the hypothesis that micelle formation occurs between T_{max} and T_{Onset} or the related concentrations. Furthermore, the authors suggest that unfolding and subsequent micelle formation start at T_{Onset} and are well advanced or completed by the time T_{max} is reached.

Poloxamers show a particular micelle formation behaviour [81,82]. While micelle formation can be multiphase for polysorbates, the highly hydrophilic P188 does not necessarily tend to micellise at room temperature and below [83,84]. As described above, surfactants with high HLB values have relatively high solubilities in the aqueous phase and relatively low surface activity. Therefore, surface saturation and micelle formation require high concentrations of P188 or elevated temperatures. According to the US and European Pharmacopeia, P188 consists of approximately 18 % PPO and 82 % PEO [85,86]. According to Griffin (1954) [11], this would give an HLB value of 16.4. However, the HLB is much higher since PPO blocks are much less hydrophobic than pure carbohydrate chains. The high percentage of PEO and low hydrophobicity of PPO leads to an HLB value of 29, calculated by an optimised method adapted from the Davies theory [12]. In general, poloxamer surfactants have been found to show a strong temperature dependence due to the high PEO content. P188 is thought to form intermolecular complexes with itself at room temperature rather than micelles composed of several molecules [1,87]. Therefore, an equilibrium between single monomers, associations of a few molecules, and micelles is suggested, as described for other poloxamers [88–90]. However, researchers have published CMC values for P188 that vary by several

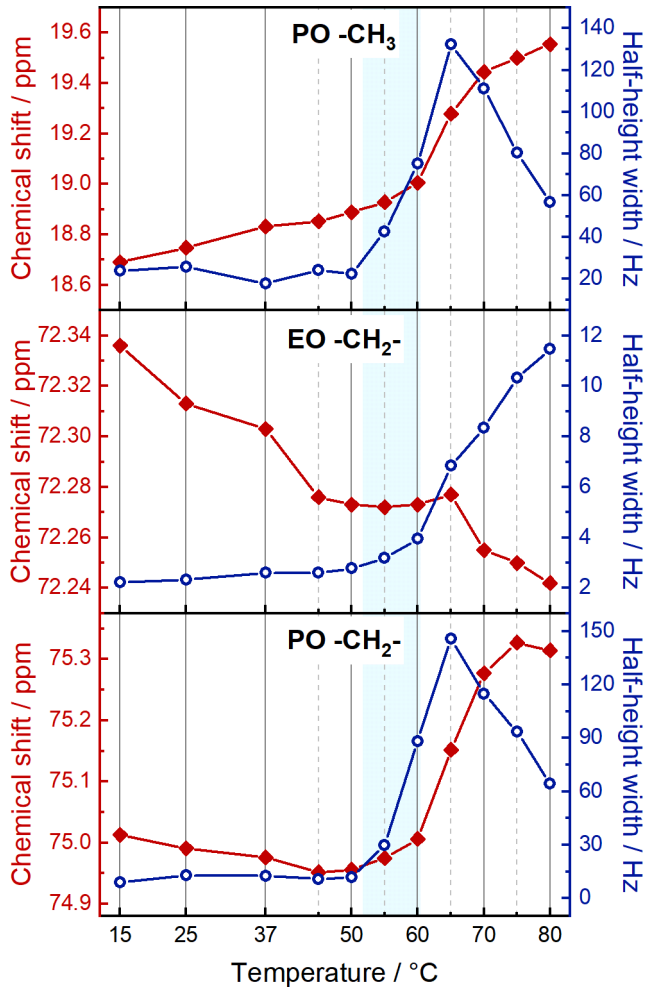

Fig. 17. Chemical shift and half-height width of the PO-CH_3, EO-CH_2- and PO-CH_2- signals in the ^{13}C-NMR spectra. Corresponding T_{max} and T_{Onset} of 40 mg·mL^{-1} are highlighted in light blue.

orders of magnitude (0.0055–10 % (w/v)) for different temperatures and conditions [4]. The main issues may be the variety of the methods used, misinterpretation of surface tension data and differences in the quality of the P188 material studied. This implies that P188 should start forming micelles at the abovementioned concentrations.

Fig. 19 shows the idealised (dotted line) surface tension versus surfactant concentration and experimental observations for P188 (solid line). Ideally, the surface tension decreases when a certain amount of surfactant is added to the solution (Fig. 19, point 1, dotted curve). The surface tension decreases sharply and may reach a local minimum (Fig. 19, point 3) due to small amounts of more hydrophobic impurities. The surface tension stabilises at an almost constant value after the air-water interface is saturated with surfactant molecules (Fig. 19, point 4). At this point, micelles are expected to form. While differences in surfactant composition and multiphase processes may cause a slower convergence to a constant value, the surface tension of P188 does not reach a plateau with increasing concentration, even at high concentrations. Therefore, published CMC values for P188 determined by surface tension measurements are often calculated as the point of decreasing slope in the logarithmic data plot [3,91]. The results obtained in this study show that no micelles are formed at this point, and the air-water interface is not fully saturated. DLS measurements support the hypothesis that intramolecular P188 associates are formed at room temperature rather than micelles composed of different surfactant monomers. Therefore, the term critical micelle concentration for P188 is misleading. Fig. 19 shows our understanding of the behaviour of P188 in an aqueous solution. As described above, P188 is thought to form intermolecular surfactant association in solution (Ia). These are in equilibrium with unfolded P188 molecules (Ib), which can saturate the surfaces with a widespread conformation (IIa). As with an idealised surfactant, the surface tension drops sharply when enough P188 molecules reach the interface (Fig. 19, solid curve, point 1). Furthermore, an increase in P188 concentration leads to a structural change of the P188 molecules and narrower accumulation at the interface (IIb). The surface tension (Fig. 19, point 2) decreases but is not as sharp as primarily (Fig. 19, point 1). At elevated temperatures, the amount of unfolded P188 is sufficient to cover the interface completely and induce micelle formation (III). The surface tension may exhibit a local minimum (Fig. 19, point 3) followed by an almost constant surface tension value (Fig. 19, point 4). This behaviour was inferred from our results for P188 in drop shape analysis, and the formation of a larger supramolecular surfactant assembly with a more hydrophobic and viscous core was demonstrated. Additionally, DSC experiments showed thermal unfolding processes in P188 solutions consistent with the expected unfolding process of intermolecular surfactant association. The micelles exhibited increased micro-viscosities in their early formation phase when they were found to contain residual water. The micelles dehydrate at higher temperatures, resulting in a non-polar PPO core “free” of water. The PEO corona does not show such a distinct behaviour but does show reduced mobility and hydrophilic interactions at higher temperatures.

As mentioned in the introduction, P188 plays a role as an excipient in protein stabilisation. Saturation of interfaces to avoid interaction of proteins with them is one of the stabilisation mechanisms discussed. Suppose surface saturation is mandatory for sufficient protein stabilisation. In that case, more than using CMC values as a benchmark for minimum concentrations is required to achieve the objective of stable biological formulations. On the other hand, P188 is also used in bioreactors to reduce cell shear stress and increase cell viability. The membrane-sealing effects of P188 have been discussed [92–94]. P188 concentrations above the CMC, as opposed to concentrations below the estimated CMC, were found to impact cell viability significantly [95]. From the perspective of our study, the reported CMC represents the first change in the slope of the surface tension (between 1 and 2 in Fig. 19, solid line) and not the point at which micelle formation begins. Thus, a complete understanding of the interfacial and micellisation behaviour of P188 is essential for formulation development and biotechnology.

5. Conclusion

The results of this work support the idea of complexity in the micelle formation behaviour of poloxamer 188 (P188). The definition of a micelle formation range rather than a single point for critical micelle temperature (CMT) and critical micelle concentration (CMC) provides a more reliable means of describing the observed effects. Various methods were found to be suitable for detecting changes in the behaviour of P188 in solution. DSC experiments defined a specific range for P188 in which micelle formation occurs. Changes in colloidal association properties, hydrophobicity, and viscosity of the formed micellar compartment were observed within this range. Variations in the proton nuclear magnetic resonance spectra indicate changes in the chemical environment of the PPO blocks, suggesting the formation of a PPO micelle core. These results are consistent with our observations from the surface tension measurements. For temperatures above 37 °C and at high surfactant concentrations in solute-rich buffers, finding a plateau in the relative surface tension plot is consistent with the theoretical considerations in which a constant surface tension indicates an excess of CMC. The findings derived from the application of these supplementary methodologies have demonstrated that the formation of a hydrophobic compartment is contingent upon the attainment of a constant surface tension value. Nevertheless, the course of the relative surface tension profile of P188

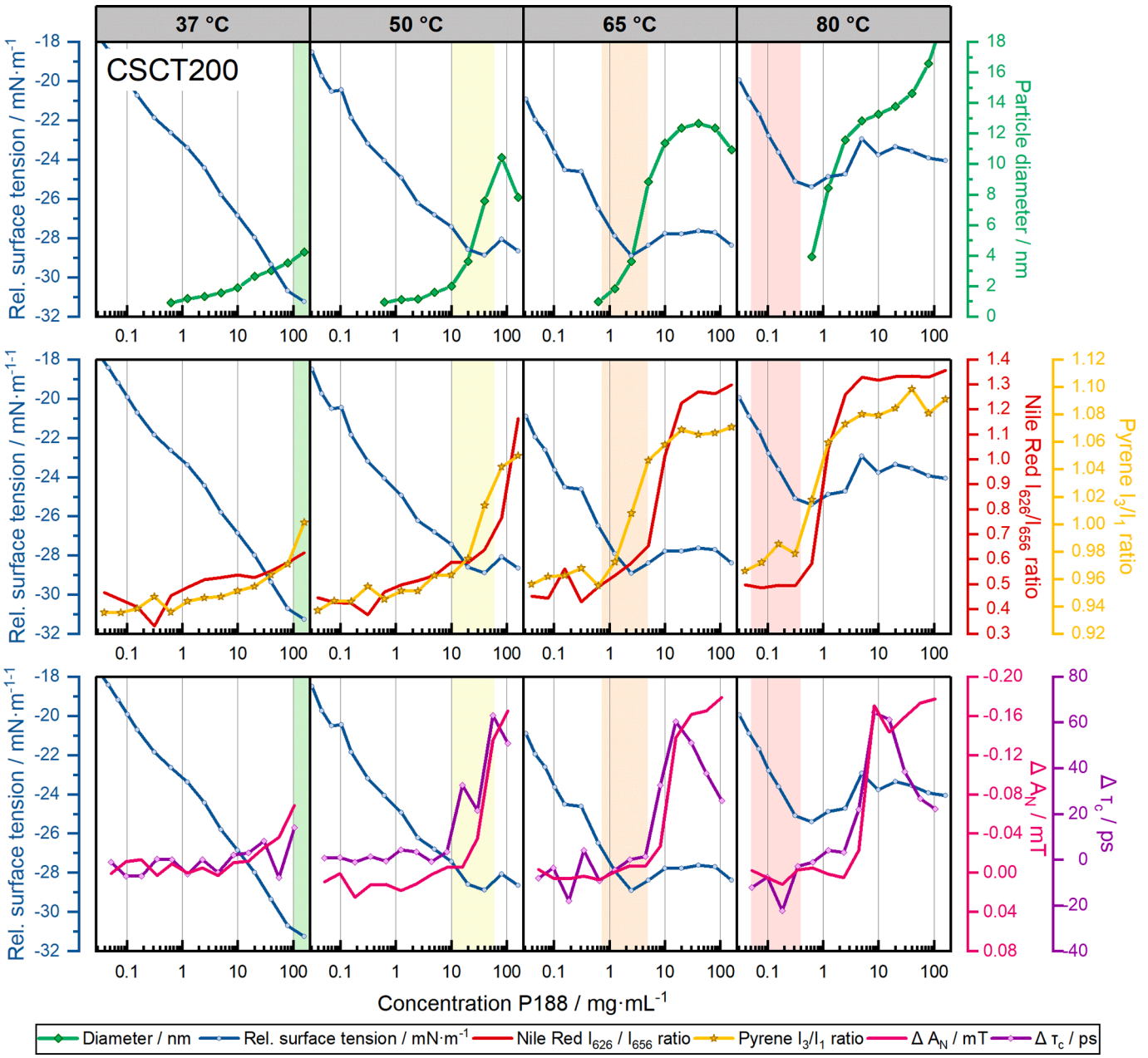

Fig. 18. Comparison of results from drop shape analysis (relative surface tension), dynamic light scattering (particle diameter), Pyrene and Nile Red fluorescence spectroscopy (intensity ratios) and electron paramagnetic resonance (EPR) spectroscopy (nitrogen isotropic hyperfine coupling constant and rotational correlation time) in Citrate buffer + 115 mM NaCl and 200 mM trehalose (CSCT200) at 37 °C, 50 °C, 65 °C and 80 °C. Concentration ranges corresponding to T_{max} and T_{Onset} are highlighted for each temperature.

appears to be different and was classified as multiphase. In contrast to the ideal CMC theory, an initial flattening of the rate of decrease of the surface tension was observed instead of reaching a constant level. Therefore, the authors assume a change in the conformation of the P188 molecules at the interface, leading to higher saturation values. The first inflection point of the relative surface tension was found to be unrelated to micelle formation and thus not appropriate for CMC determination. The CMC values can be lowered by increasing temperatures and adding anti-chaotropic solutes. Overall, the investigations for P188 in water showed that temperatures above 37 °C are essential for micelle formation. Therefore, the concept of a critical micelle concentration at formulation-relevant conditions for proteins (room temperature and below) is misleading. Micelle formation, however, can be expected for non-protein formulation technologies, which often include a heating step or unintended, process immanent temperature increases (e.g. milling, high-pressure homogenisation). In currently approved pharmaceutical formulations, the concentrations of P188 range from 0.01 to 8.0 mg·mL^{-1} [4]. Orencia®, containing abatacept, is formulated with 8.0 mg·mL^{-1} P188 along with 170 mg·mL^{-1} sucrose and approximately 1 mg·mL^{-1} phosphate buffer [96]. Assuming 25 mM citrate buffer with 115 mM sodium chloride and 200 mM trehalose (CSCT200) to be the formulation's most analogous buffer system, we expect micelles to form above 65 °C. Therefore, whether changes in the interfacial behaviour of P188 are reasonable for differences in the stabilisation properties for proteins, cells, or viral vectors should be investigated in more detail.

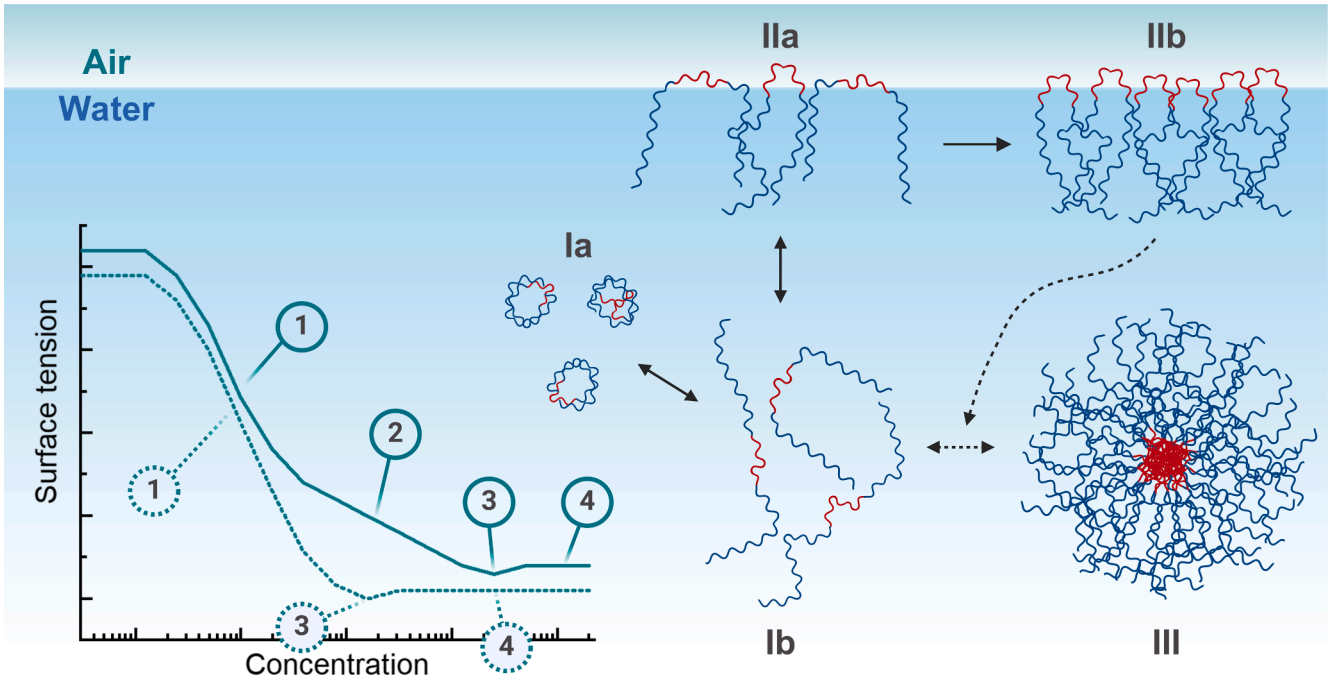

Fig. 19. Proposed behaviour of P188 in aqueous solution and at the water–air interface. Theoretical surface tension curves are depicted for idealised surfactant behaviour (dotted line) and P188 (solid line) to highlight the multi-phase behaviour. The phases of surface tension highlighted by the arabic numbers 1–4 are described in the text. P188 molecules can be present as intermolecular associations (Ia) or unfolded molecules (Ib). P188 interacts with the water–air interface at low concentrations, decreasing relative surface tension (IIa). After a first saturation of the surface by spread molecules, a further increase in concentration leads to an increase of the surfactant at the water–air interface, deformation of the molecules, and thus further saturation of the surface [69–71]. If the interface is saturated and no further deformation of molecules is possible, micelle formation is assumed (III).

CRediT authorship contribution statement

Lukas Bollenbach: Writing – review & editing, Writing – original draft, Visualization, Validation, Investigation, Formal analysis, Conceptualization. **Marie-Luise Trutschel:** Writing – review & editing, Software, Formal analysis. **Stefan Gröger:** Writing – review & editing, Investigation. **Patrick Garidel:** Writing – review & editing, Supervision, Resources, Project administration, Conceptualization. **Karsten Mäder:** Writing – review & editing, Supervision, Resources, Project administration, Conceptualization.

Declaration of competing interest

The authors declare the following financial interests/personal relationships which may be considered as potential competing interests: Lukas Bollenbach reports financial support was provided by Boehringer Ingelheim GmbH. Karsten Maeder reports financial support was provided by Boehringer Ingelheim GmbH. Patrick Garidel reports a relationship with Boehringer Ingelheim GmbH that includes: employment. If there are other authors, they declare that they have no known competing financial interests or personal relationships that could have appeared to influence the work reported in this paper.

Acknowledgement

We thank Tim Diederichs, Torsten Schultz-Fademrecht, Julia Buske (Boehringer Ingelheim), Johanna Weber, and Daniel Brucks (Martin-Luther-University Halle-Wittenberg) for discussing the experimental design and results. Holger Thie is acknowledged for excellent support in project management. Special thanks go to Florian Lehmann (AG Hinderberger, Martin-Luther-University Halle-Wittenberg) for the support in EPR experiments and Andrea Eiperle (Boehringer Ingelheim) for the support in DSC experiments. The authors would like to thank Sophie Bollenbach for proofreading the manuscript. The graphical abstract and Fig. 19 were generated using a licensed version of biorender.com.

Data availability

Data will be made available on request.

References

[1] I.R. Schmolka, A Review of Block Polymer Surfactants, J. Am. Oil Chem. Soc. 54 (1977) 110–116, https://doi.org/10.1007/BF02894385.
[2] P. Alexandridis, T. Alan Hatton, Poly(ethylene oxide)poly(propylene oxide)poly (ethylene oxide) Block Copolymer Surfactants in Aqueous Solutions and at Interfaces: Thermodynamics, Structure, Dynamics, and Modeling, Colloids Surfaces A Physicochem. Eng. Asp. 96 (1995) 1–46, https://doi.org/10.1016/0927-7757(94)03028-X.
[3] K.N. Prasad, T.T. Luong, A.T. FlorenceJoelle Paris, C. Vaution, M. Seiller, F. Puisieux, Surface Activity and Association of ABA Polyoxyethylene—polyoxypropylene Block Copolymers in Aqueous Solution, J. Colloid Interface Sci. 69 (1979) 225–232, https://doi.org/10.1016/0021-9797(79)90151-6.
[4] L. Bollenbach, J. Buske, K. Mäder, P. Garidel, Poloxamer 188 as Surfactant in Biological Formulations – An Alternative for Polysorbate 20/80? Int. J. Pharm. 620 (2022) 121706 https://doi.org/10.1016/j.ijpharm.2022.121706.
[5] IUPAC, Critical Micelle Concentration (CMC), IUPAC Compend. Chem. Terminol. 1077 (2008) 2014. Doi: 10.1351/goldbook.c01395.
[6] M.T. Lee, A. Vishnyakov, A.V. Neimark, Calculations of Critical Micelle Concentration by Dissipative Particle Dynamics Simulations: The Role of Chain Rigidity, J. Phys. Chem. B 117 (2013) 10304–10310, https://doi.org/10.1021/jp4042028.
[7] G.M. Wilmes, D.J. Arnold, K.S. Kawchak, Effect of Chain Rigidity on Block Copolymer Micelle Formation and Dissolution as Observed by 1H-NMR Spectroscopy, J. Polym. Res. 18 (2011) 1787–1797, https://doi.org/10.1007/s10965-011-9585-7.
[8] J. Hu, S.E. Anachkov, T. Moaddel, J.O. Carnali, Reexamining the Enhanced Solubility of Sodium Laurate/Sodium Oleate Eutectic Mixtures, Langmuir (2025), https://doi.org/10.1021/acs.langmuir.4c02919.
[9] M.E. Mahmood, D.A.F. Al-koofee, Effect of Temperature Changes on Critical Micelle Concentration for Tween Series Surfactant, Glob. J. Sci. Front. Res. Chem. 13 (2013) 1–7.
[10] T. Menzen, W. Friess, High-Throughput Melting-Temperature Analysis of a Monoclonal Antibody by Differential Scanning Fluorimetry in the Presence of

Surfactants, J. Pharm. Sci. 102 (2013) 415–428, https://doi.org/10.1002/jps.23405.
[11] W.C. Griffin, Calculation of HLB Values of Non-ionic Surfactants, J. Soc. Cosmet. Chem. 5 (1954).
[12] X. Guo, Z. Rong, X. Ying, Calculation of Hydrophile-lipophile Balance for Polyethoxylated Surfactants by Group Contribution Method, J. Colloid Interface Sci. 298 (2006) 441–450, https://doi.org/10.1016/j.jcis.2005.12.009.
[13] R.C. Pasquali, M.P. Taurozzi, C. Bregni, Some Considerations about the Hydrophilic-Lipophilic Balance System, Int. J. Pharm. 356 (2008) 44–51, https://doi.org/10.1016/j.ijpharm.2007.12.034.
[14] P. Linse, M. Malmsten, Temperature-Dependent Micellization in Aqueous Block Copolymer Solutions, Macromolecules 25 (1992) 5434–5439, https://doi.org/10.1021/ma00046a048.
[15] E. Fisicaro, C. Compari, A. Braibanti, Entropy/Enthalpy Compensation: Hydrophobic Effect, Micelles and Protein Complexes, PCCP 6 (2004) 4156–4166, https://doi.org/10.1039/b404327h.
[16] L.J. Chen, S.Y. Lin, C.C. Huang, Effect of Hydrophobic Chain Length of Surfactants on Enthalpy-Entropy Compensation of Micellization, J. Phys. Chem. B 102 (1998) 4350–4356, https://doi.org/10.1021/jp9804345.
[17] T. Wu, H. Liu, Role of Isomers and Steric Hindrance in the Micellization of Carboxylated Carbosilane Surfactants, (2024) 1–11. Doi: 10.1002/jsde.12744.
[18] A. Bera, S. Kumar, A. Mandal, Temperature-dependent Phase Behavior, Particle Size, and Conductivity of Middle-phase Microemulsions Stabilized by Ethoxylated Nonionic Surfactants, J. Chem. Eng. Data 57 (2012) 3617–3623, https://doi.org/10.1021/je300845q.
[19] L.J. Chen, S.Y. Lin, C.C. Huang, E.M. Chen, Temperature Dependence of Critical Micelle Concentration of Polyoxyethylenated Non-ionic Surfactants, Colloids Surfaces A Physicochem. Eng. Asp. 135 (1998) 175–181, https://doi.org/10.1016/S0927-7757(97)00238-0.
[20] N. Scholz, T. Behnke, U. Resch-Genger, Determination of the Critical Micelle Concentration of Neutral and Ionic Surfactants with Fluorometry, Conductometry, and Surface Tension—A Method Comparison, J. Fluoresc. 28 (2018) 465–476, https://doi.org/10.1007/s10895-018-2209-4.
[21] S.Y. Lin, A Study of the Equilibrium Surface Tension and the Critical Micelle Concentration of Mixed Surfactant Solutions, Langmuir 15 (1999) 4370–4376, https://doi.org/10.1021/la981149f.
[22] K.J. Mysels, Surface Tension of Solutions of Pure Sodium Dodecyl Sulfate, Langmuir 2 (1986) 423–428, https://doi.org/10.1021/la00070a008.
[23] K.J. Mysels, R.E. Stafford, Time and Concentration Resolved Surface Tension, Colloids Surf. 51 (1990) 105–114, https://doi.org/10.1016/0166-6622(90)80135-Q.
[24] S.A. Tabak, R.H. Notter, J.S. Ultman, S.M. Dinh, Relaxation Effects in the Surface Pressure Behavior of Dipalmitoyl Lecithin, J. Colloid Interface Sci. 60 (1977) 117–125, https://doi.org/10.1016/0021-9797(77)90262-4.
[25] J.K. Salem, I.M. El-Nahhal, S.F. Salama, Determination of the Critical Micelle Concentration by Absorbance and Fluorescence Techniques using Fluorescein Probe, Chem. Phys. Lett. 730 (2019) 445–450, https://doi.org/10.1016/j.cplett.2019.06.038.
[26] K. Lee, S.C. Shin, I. Oh, Fluorescence Spectroscopy Studies on Micellization of Poloxamer 407 Solution, Arch. Pharm. Res. 26 (2003) 653–658, https://doi.org/10.1007/BF02976716.
[27] P.R. Majhi, A. Blume, Thermodynamic Characterization of Temperature-induced Micellization and Demicellization of Detergents Studied by Differential Scanning Calorimetry, Langmuir 17 (2001) 3844–3851, https://doi.org/10.1021/la001660k.
[28] P. Alexandridis, J.F. Holzwarth, Differential Scanning Calorimetry Investigation of the Effect of Salts on Aqueous Solution Properties of an Amphiphilic Block Copolymer (Poloxamer), Langmuir 13 (1997) 6074–6081, https://doi.org/10.1021/la9703712.
[29] S. Gaisford, A.E. Beezer, J.C. Mitchell, P.C. Bell, F. Fakorede, J.K. Finnie, S. J. Williams, Temperature Induced Aggregation in Aqueous Solution of a Series of PEO-PPO-PEO Copolymers, Int. J. Pharm. 174 (1998) 39–46, https://doi.org/10.1016/S0378-5173(98)00223-3.
[30] R.K. Thapa, F. Cazzador, K.G. Grønlien, H.H. Tønnesen, Effect of Curcumin and Cosolvents on the Micellization of Pluronic F127 in Aqueous Solution, Colloids Surfaces B Biointerfaces. 195 (2020) 111250, https://doi.org/10.1016/j.colsurfb.2020.111250.
[31] P. Alexandridis, T. Nivaggioli, T.A. Hatton, Temperature Effects on Structural Properties of Pluronic P104 and F108 PEO-PPO-PEO Block Copolymer, Solutions 35 (1995) 1468–1476.
[32] S. Bhattacharjee, S. Pandit, D. Seth, How Kosmotropic and Chaotropic Osmolytes Perturb the Properties of an Aqueous Solution of a Pluronic Block Copolymer? Langmuir 38 (2022) 9347–9362, https://doi.org/10.1021/acs.langmuir.2c01207.
[33] Z. Zhou, B. Chu, Light-scattering Study on the Association Behavior of Triblock Polymers of Ethylene Oxide and Propylene Oxide in Aqueous Solution, J. Colloid Interface Sci. 126 (1988) 171–180, https://doi.org/10.1016/0021-9797(88)90111-7.
[34] G. Cerichelli, G. Mancinit, NMR Techniques Applied to Micellar Systems, Curr. Opin. Colloid Interface Sci. 2 (1997) 641–648, https://doi.org/10.1016/s1359-0294(97)80058-1.
[35] M. Florent, R. Shvartzman-Cohen, D. Goldfarb, R. Yerushalmi-Rozen, Self-Assembly of Pluronic Block Copolymers in Aqueous Dispersions of Single-wall Carbon Nanotubes as Observed by Spin Probe EPR, Langmuir 24 (2008) 3773–3779, https://doi.org/10.1021/la7037922.
[36] S. Ruthstein, A. Potapov, A.M. Raitsimring, D. Goldfarb, Double Electron Electron Resonance as a Method for Characterization of Micelles, J. Phys. Chem. B 109 (2005) 22843–22851, https://doi.org/10.1021/jp054450v.
[37] J. Ma, C. Guo, Y. Tang, J. Wang, L. Zheng, X. Liang, S. Chen, H. Liu, Microenvironmental and Conformational Structure of Triblock Copolymers in Aqueous Solution by 1H and 13C NMR Spectroscopy, J. Colloid Interface Sci. 299 (2006) 953–961, https://doi.org/10.1016/j.jcis.2006.02.021.
[38] C.S. Klug, J.B. Feix, Methods and Applications of Site-directed Spin Labeling EPR, Spectroscopy (2008), https://doi.org/10.1016/S0091-679X(07)84020-9.
[39] A.M. Tedeschi, G. D'Errico, E. Busi, R. Basosi, V. Barone, Micellar Aggregation of Sulfonate Surfactants Studied by Electron Paramagnetic Resonance of a Cationic Nitroxide: An Experimental and Computational Approach, PCCP 4 (2002) 2180–2188, https://doi.org/10.1039/b106833d.
[40] A.M. Tedeschi, E. Busi, L. Paduano, R. Basosi, G. D'Errico, Influence of the Headgroup Molecular Structure on the Anionic Surfactant-PVP Interaction Studied by Electron Paramagnetic Resonance of a Cationic Nitroxide, PCCP 5 (2003) 5077–5083, https://doi.org/10.1039/b305739a.
[41] P. Garidel, M. Blech, J. Buske, A. Blume, Surface Tension and Self-association Properties of Aqueous Polysorbate 20 HP and 80 HP Solutions: Insights into Protein Stabilisation Mechanisms, J. Pharm. Innov. (2020), https://doi.org/10.1007/s12247-020-09488-4.
[42] H.J. Lee, A. McAuley, K.F. Schilke, J. McGuire, Molecular Origins of Surfactant-mediated Stabilization of Protein Drugs, Adv. Drug Deliv. Rev. 63 (2011) 1160–1171, https://doi.org/10.1016/j.addr.2011.06.015.
[43] X. Yuan, S. Krueger, E. Shalaev, Protein-Surfactant and Protein-Protein Interactions During Freeze and Thaw: A Small-Angle Neutron Scattering Study of Lysozyme Solutions with Polysorbate and Poloxamer, J. Pharm. Sci. 112 (2023) 76–82, https://doi.org/10.1016/j.xphs.2022.08.017.
[44] G.E. Yu, H. Altinok, S.K. Nixon, C. Booth, P. Alexandridis, T.A. Hatton, Self-association properties of oxyethylene/oxypropylene/oxyethylene triblock copolymer F88, Eur. Polym. J. 33 (1997) 673–677, https://doi.org/10.1016/S0014-3057(96)00194-2.
[45] P. Alexandridis, J.F. Holzwarth, T.A. Hatton, Micellization of Poly(ethylene oxide)-Poly(propylene oxide)-Poly(ethylene oxide) Triblock Copolymers in Aqueous Solutions: Thermodynamics of Copolymer Association, Macromolecules 27 (1994) 2414–2425, https://doi.org/10.1021/ma00087a009.
[46] P. Alexandridis, J.F. Holzwarth, T. Alan Hatton, A Correlation for the Estimation of Critical Micellization Concentrations and Temperatures of Polyols in Aqueous Solutions, J. Am. Oil Chem. Soc. 72 (1995) 823–826, https://doi.org/10.1007/BF02541032.
[47] S. Stoll, A. Schweiger, EasySpin, a Comprehensive Software Package for Spectral Simulation and Analysis in EPR, J. Magn. Reson. 178 (2006) 42–55, https://doi.org/10.1016/j.jmr.2005.08.013.
[48] H. Knoch, M.H. Ulbrich, J.J. Mittag, J. Buske, P. Garidel, H. Heerklotz, Complex Micellization Behavior of the Polysorbates Tween 20 and Tween 80, Mol. Pharm. 18 (2021) 3147–3157, https://doi.org/10.1021/acs.molpharmaceut.1c00406.
[49] L. Magnus Bergström, Second CMC in Surfactant Micellar Systems, Curr. Opin. Colloid Interface Sci. 22 (2016) 46–50, https://doi.org/10.1016/j.cocis.2016.02.008.
[50] I. Paterson, J. Armstrong, B. Chowdhry, S. Leharne, Thermodynamic Model Fitting of the Calorimetric Output Obtained for Aqueous Solutions of Oxyethylene-oxypropylene-oxyethylene Triblock Copolymers, Langmuir 13 (1997) 2219–2226, https://doi.org/10.1021/la960432g.
[51] G. Wanka, H. Hoffmann, W. Ulbricht, Phase Diagrams and Aggregation Behavior of Poly(oxyethylene)-Poly(oxypropylene)-Poly(oxyethylene) Triblock Copolymers in Aqueous Solutions, Macromolecules 27 (1994) 4145–4159, https://doi.org/10.1021/ma00093a016.
[52] J.K. Armstrong, J. Parsonage, B. Chowdhry, S. Leharne, J. Mitchell, A. Beezer, K. Loehner, P. Laggner, Scanning Densitometric and Calorimetric Studies of Poly (ethylene oxide)/Poly(propylene oxide)/Poly(ethylene oxide) Triblock Copolymers (Poloxamers) in Dilute Aqueous Solution, J. Phys. Chem. 97 (1993) 3904–3909, https://doi.org/10.1021/j100117a042.
[53] H.X. Zhou, Interactions of Macromolecules with Salt Ions: An Electrostatic Theory for the Hofmeister Effect, Proteins Struct. Funct. Genet. 61 (2005) 69–78, https://doi.org/10.1002/prot.20500.
[54] K. Patel, B. Bharatiya, Y. Kadam, P. Bahadur, Micellization and Clouding Behavior of EO-PO Block Copolymer in Aqueous Salt Solutions, J. Surfactant Deterg. 13 (2010) 89–95, https://doi.org/10.1007/s11743-009-1127-5.
[55] D. Patel, R. Jana, M.H. Lin, K. Kuperkar, D. Seth, L.J. Chen, P. Bahadur, Revisiting the Salt-triggered Self-assembly in very Hydrophilic Triblock Copolymer Pluronic® F88 Using Multitechnique Approach, Colloid Polym. Sci. 299 (2021) 1113–1126, https://doi.org/10.1007/s00396-021-04833-6.
[56] C. Branca, S. MacCarrone, S. Magazu, G. Maisano, S.M. Bennington, J. Taylor, Tetrahedral Order in Homologous Disaccharide-Water Mixtures, J. Chem. Phys. 122 (2005), https://doi.org/10.1063/1.1887167.
[57] M. Kaszuba, D. McKnight, M.T. Connah, F.K. McNeil-Watson, U. Nobbmann, Measuring Sub Nanometre Sizes Using Dynamic Light Scattering, J. Nanoparticle Res. 10 (2008) 823–829, https://doi.org/10.1007/s11051-007-9317-4.
[58] E. Russo, C. Villa, Poloxamer Hydrogels for Biomedical Applications, Pharmaceutics. 11 (2019), https://doi.org/10.3390/pharmaceutics11120671.
[59] I.N. Kurniasih, H. Liang, P.C. Mohr, G. Khot, J.P. Rabe, A. Mohr, Nile Red Dye in Aqueous Surfactant and Micellar Solution, Langmuir 31 (2015) 2639–2648, https://doi.org/10.1021/la504378m.
[60] J.R. Daban, M. Samsó, S. Bartolomé, Use of Nile Red as a Fluorescent Probe for the Study of the Hydrophobic Properties of Protein-Sodium Dodecyl Sulfate Complexes

in Solution, Anal. Biochem. 199 (1991) 162–168, https://doi.org/10.1016/0003-2697(91)90084-7.
[61] National Library of Medicine, Nile Red – Chemical and Physical Properties, (2021). https://pubchem.ncbi.nlm.nih.gov/compound/Nile-red#section=Chemical-and-Physical-Properties (accessed May 2, 2024).
[62] P. Greenspan, S.D. Fowler, Spectrofluorometric Studies of the Lipid Probe, Nile Red, J. Lipid Res. 26 (1985) 781–789, https://doi.org/10.1016/s0022-2275(20)34307-8.
[63] K. Kalyanasundaram, J.K. Thomas, Environmental Effects on Vibronic Band Intensities in Pyrene Monomer Fluorescence and Their Application in Studies of Micellar Systems, J. Am. Chem. Soc. 99 (1977) 2039–2044, https://doi.org/10.1021/ja00449a004.
[64] J. Aguiar, P. Carpena, J.A. Molina-Bolívar, C. Carnero Ruiz, On the Determination of the Critical Micelle Concentration by the Pyrene 1:3 Ratio Method, J. Colloid Interface Sci. 258 (2003) 116–122, https://doi.org/10.1016/S0021-9797(02)00082-6.
[65] A.V. Kabanov, I.R. Nazarova, I.V. Astafieva, E.V. Batrakova, V.Y. Alakhov, A. A. Yaroslavov, V.A. Kabanov, Micelle Formation and Solubilization of Fluorescent Probes in Poly(oxyethylene-6-oxypropylene-6-oxyethylene) Solutions, Macromolecules 28 (1995) 2303–2314, https://doi.org/10.1021/ma00111a026.
[66] D.L. Sackett, J. Wolff, Nile Red as a Polarity-sensitive Fluorescent Probe of Hydrophobic Protein Surfaces, Anal. Biochem. 167 (1987) 228–234, https://doi.org/10.1016/0003-2697(87)90157-6.
[67] V. Glushko, M.S.R. Thaler, C.D. Karp, Pyrene Fluorescence Fine Structure Hydrophobic Regions : Behavior as a Polarity Probe of in Model Solvents ' regions play a key role in of membranes and con- polar groups from the aqueous phase into has been de- driven process that depends to and protein, Arch. Biochem. Biophys. 210 (1981) 33–42.
[68] M. Balcan, D.F. Anghel, V. Raicu, Phase Behavior of Water/Oil/Nonionic Surfactants with Normal Distribution of the Poly(ethylene oxide) Chain Length, Colloid Polym. Sci. 281 (2003) 143–149, https://doi.org/10.1007/s00396-002-0755-3.
[69] G.L. Jaime, S.M. Isabel, C. Angel, A.L. Carmen, Poloxamines and Poloxamers as Polymeric Micellar Carriers for Simvastatin: Interactions at the Air-Water Interface and in Bulk Solution, J. Phys. Chem. C 114 (2010) 1181–1189, https://doi.org/10.1021/jp9094358.
[70] C. Chen, M.A. Even, Z. Chen, Detecting Molecular-Level Chemical Structure and Group Orientation of Amphiphilic PEO-PPO-PEO Copolymers at Solution/Air and Solid/Solution Interfaces by SFG Vibrational Spectroscopy, Macromolecules 36 (2003) 4478–4484, https://doi.org/10.1021/ma025985e.
[71] M.G. Muñoz, F. Monroy, F. Ortega, R.G. Rubio, D. Langevin, Monolayers of Symmetric Triblock Copolymers at the Air-Water Interface. 1. Equilibrium Properties, Langmuir 16 (2000) 1083–1093, https://doi.org/10.1021/la990142a.
[72] B.R. Knauer, J.J. Napier, Splitting of Nitroxide (1975) 4395–4400.
[73] N. Beghein, L. Rouxhet, M. Dinguizli, M.E. Brewster, A. Ariën, V. Préat, J.L. Habib, B. Gallez, Characterization of Self-Assembling Copolymers in Aqueous Solutions Using Electron Paramagnetic Resonance and Fluorescence Spectroscopy, J. Control. Release 117 (2007) 196–203, https://doi.org/10.1016/j.jconrel.2006.10.028.
[74] M. Vasilescu, R. Bandula, H. Lemmetyinen, Micropolarity and Microviscosity of Pluronics L62 and L64 Core-shell Aggregates in Water at Various Concentrations and Additives Examined by Absorption and Fluorescence Probes, Colloid Polym. Sci. 288 (2010) 1173–1184, https://doi.org/10.1007/s00396-010-2247-1.
[75] O. Annunziata, L. Costantino, G. D'Errico, L. Paduano, V. Vitagliano, Transport Properties for Aqueous Sodium Sulfonate Surfactants, J. Colloid Interface Sci. 216 (1999) 16–24, https://doi.org/10.1006/jcis.1999.6269.
[76] J. Hao, T. Wang, S. Shi, R. Lu, H. Wang, Electron Spin Resonance Study of Effect of Urea on Microenvironmental Properties of Alkylbenzenesulfonate Micellar Solutions, Langmuir 13 (1997) 1897–1900, https://doi.org/10.1021/la9604442.
[77] J.H. Ma, C. Guo, Y.L. Tang, H.Z. Liu, 1H NMR Spectroscopic Investigations on the Micellization and Gelation of PEO-PPO-PEO Block Copolymers in Aqueous Solutions, Langmuir 23 (2007) 9596–9605, https://doi.org/10.1021/la701221f.
[78] B.J. Kim, S.S. Im, S.G. Oh, Investigation on the Solubilization Locus of Aniline-HCl Salt in SDS Micelles with 1H NMR Spectroscopy, Langmuir 17 (2001) 565–566, https://doi.org/10.1021/la0012889.
[79] C. Guo, J. Wang, H.Z. Liu, J.Y. Chen, Hydration and Conformation of Temperature-dependent Micellization of PEO-PPO-PEO Block Copolymers in Aqueous Solutions by FT-Raman, Langmuir 15 (1999) 2703–2708, https://doi.org/10.1021/la981036w.
[80] C. Guo, H.Z. Liu, J.Y. Chen, A Fourier Transform Infrared Study of the Phase Transition in Aqueous Solutions of Ethylene Oxide-Propylene Oxide Triblock Copolymer, Colloid Polym. Sci. 277 (1999) 376–381, https://doi.org/10.1007/s003960050395.
[81] G. Buckton, E.O. Machiste, Differences between Dynamic and Equilibrium Surface Tension of Poly(oxyethylene)-Poly(oxypropylene)-Poly(oxyethylene) Block Copolymer Surfactants (Poloxamers P407, P237, and P338) in Aqueous Solution, J. Pharm. Sci. 86 (1997) 163–166, https://doi.org/10.1021/js960343o.
[82] Z. Zhou, B. Chu, Anomalous Micellization Behavior and Composition Heterogeneity of a Triblock ABA Copolymer of (A) Ethylene Oxide and (B) Propylene Oxide in Aqueous Solution, Macromolecules 21 (1988) 2548–2554, https://doi.org/10.1021/ma00186a039.
[83] R.R. Ford, P.H. Gilbert, R. Gillilan, Q. Huang, R. Donnelly, K.K. Qian, D.P. Allen, N. J. Wagner, Y. Liu, Micelle Formation and Phase Separation of Poloxamer 188 and Preservative Molecules in Aqueous Solutions Studied by Small Angle X-ray Scattering, J. Pharm. Sci. 112 (2023) 731–739, https://doi.org/10.1016/j.xphs.2022.09.019.
[84] J. Molpeceres, M. Guzmán, P. Bustamante, M. Del Rosario Aberturas, Exothermic-Endothermic Heat of Solution Shift of Cyclosporin A Related to Poloxamer 188 Behavior in Aqueous Solutions, Int. J. Pharm. 130 (1996) 75–81, https://doi.org/10.1016/0378-5173(95)04294-6.
[85] United States Pharmacopeial Convention, Monograph Poloxamer, USP 43 - NF 38. (2020). https://online.uspnf.com/uspnf/document/1_GUID-E49EC74D-A009-459A-820B-5DEE801E2FBF_4_en-US.
[86] Deutscher Apotheker Verlag, Arzneibuchmonografie 10.0/1464 - Poloxamere Poloxamera, Eur. Arzneib. (2020) 5358–5360.
[87] I.R. Schmolka, A.J. Raymond, Micelle Formation of Polyoxyethylene-Polyoxypropylene Surfactants, J. Am. Oil Chem. Soc. 42 (1965) 1088–1091, https://doi.org/10.1007/BF02636916.
[88] W. Brown, K. Schillen, M. Almgren, S. Hvidt, P. Bahadur, Micelle and Gel Formation in a Poly(ethylene oxide)/Poly(propylene oxide)/Poly(ethylene oxide) Triblock Copolymer in Water Solution: Dynamic and Static Light Scattering and Oscillatory Shear Measurements, J. Phys. Chem. 95 (1991) 1850–1858, https://doi.org/10.1021/j100157a064.
[89] M. Almgren, W. Brown, S. Hvidt, Self-Aggregation and Phase Behavior of Poly (ethylene oxide)-Poly(propylene oxide)-poly(ethylene oxide) Block Copolymers in Aqueous Solution, Colloid Polym. Sci. 273 (1995) 2–15, https://doi.org/10.1007/BF00655668.
[90] S. Hvidt, W. Batsberg, Characterization and Micellization of a Poloxamer Block Copolymer, Int. J. Polym. Anal. Charact. 12 (2007) 13–22, https://doi.org/10.1080/10236660601094093.
[91] W. Saski, S.G. Shah, Availability of Drugs in the Presence of Surface-active Agents I Critical Micelle Concentrations of some Oxyethylene Oxypropylene Polymers, J. Pharm. Sci. 54 (1965) 71–74, https://doi.org/10.1002/jps.2600540117.
[92] S.A. Maskarinec, G. Wu, K.Y.C. Lee, Membrane Sealing by Polymers, Ann. N. Y. Acad. Sci. 1066 (2006) 310–320, https://doi.org/10.1196/annals.1363.018.
[93] H. Chen, C. McFaul, I. Titushkin, M. Cho, R. Lee, Surfactant Copolymer Annealing of Chemically Permeabilized Cell Membranes, Regen. Eng. Transl. Med. 4 (2018) 1–10, https://doi.org/10.1007/s40883-017-0044-9.
[94] F.A. Merchant, W.H. Holmes, M. Capelli-Schellpfeffer, R.C. Lee, M. Toner, Poloxamer 188 Enhances Functional Recovery of Lethally Heat-Shocked Fibroblasts, J. Surg. Res. 74 (1998) 131–140, https://doi.org/10.1006/jsre.1997.5252.
[95] V.D. Samith, G. Miño, E. Ramos-Moore, N. Arancibia-Miranda, Effects of Pluronic F68 Micellization on the Viability of Neuronal Cells in Culture, J. Appl. Polym. Sci. 130 (2013) 2159–2164, https://doi.org/10.1002/app.39426.
[96] U.S. Food and Drug Administration, Full Prescribing Information: Orencia®, (2023). https://dailymed.nlm.nih.gov/dailymed/drugInfo.cfm?setid=0836c6ac-ee37-5640-2fed-a3185a0b16eb (accessed May 2, 2024).